

A sparse spectral method for fractional differential equations in one-spacial dimension

Ioannis P. A. Papadopoulos* Sheehan Olver†

October 18, 2022

Abstract

We develop a sparse spectral method for a class of fractional differential equations, posed on \mathbb{R} , in one dimension. These equations can include sqrt-Laplacian, Hilbert, derivative and identity terms. The numerical method utilizes a basis consisting of weighted Chebyshev polynomials of the second kind in conjunction with their Hilbert transforms. The former functions are supported on $[-1, 1]$ whereas the latter have global support. The global approximation space can contain different affine transformations of the basis, mapping $[-1, 1]$ to other intervals. Remarkably, not only are the induced linear systems sparse, but the operator decouples across the different affine transformations. Hence, the solve reduces to solving K independent sparse linear systems of size $\mathcal{O}(n) \times \mathcal{O}(n)$, with $\mathcal{O}(n)$ nonzero entries, where K is the number of different intervals and n is the highest polynomial degree contained in the sum space. This results in an $\mathcal{O}(n)$ complexity solve. Applications to fractional heat and wave equations are considered.

1 Introduction

In this work, we develop a spectral method to solve equations of the form

$$\mathcal{L}_{\lambda,\mu,\eta}[u] := (\lambda\mathcal{I} + \mu\mathcal{H} + \eta\frac{d}{dx} + (-\Delta)^{1/2})[u] = f, \quad (\star)$$

*Department of Mathematics, Imperial College London, UK.

`ioannis.papadopoulos13@imperial.ac.uk`,

†Department of Mathematics, Imperial College London, UK, `s.olver@imperial.ac.uk`.

Funding: This work was completed with the support of the EPSRC grant EP/T022132/1 “Spectral element methods for fractional differential equations, with applications in applied analysis and medical imaging” and the Leverhulme Trust Research Project Grant RPG-2019-144 “Constructive approximation theory on and inside algebraic curves and surfaces”.

in one dimension where $\lambda, \mu, \eta \in \mathbb{R}$ are known constants, \mathcal{H} is the Hilbert transform and $(-\Delta)^{1/2}$ is the sqrt-Laplacian, as defined in the next section. The domain is the whole real line \mathbb{R} . We seek a solution such that:

$$\lim_{|x| \rightarrow \infty} u(x) = 0. \quad (1.1)$$

Equations of the form (\star) arise in several contexts. For instance when $\lambda = \eta = \mu = 0$ and $\lambda = 1, \eta = \mu = 0$ we recover the fractional Poisson and fractional (positive-definite) Helmholtz problem, respectively. Such equations have found many uses [4, 7, 14, 22, 24]. In particular the fractional Helmholtz equation arises after a backward Euler time discretization of equations such as the fractional heat equation

$$\partial_t u(x, t) + (-\Delta)^{1/2}[u](x, t) = f(x, t). \quad (1.2)$$

In this case, the constant $\lambda = (\Delta t)^{-1}$ is the inverse of the time step size and $\mu = \eta = 0$. It also arises in power law absorption [44] or during the Newton linearization for nonlocal Burgers-type equations [6, 18], which have applications for quasi-geostrophic equations [15], or fractional porous medium flow [13].

Our approach is to approximate the function u with a space of functions consisting of weighted Chebyshev polynomials of the second kind and their Hilbert transforms, the span of which we refer to as a *sum space*: it is a direct sum of the span of two orthogonal bases. This approach is inspired by a similar method utilized by Hale and Olver for fractional integral and differential equations [23]. As the Hilbert transform is an anti-involution, $\mathcal{H}[\mathcal{H}[u]] = -u$, the operator $(\lambda\mathcal{I} + \mathcal{H})$ maps the sum space to itself and the operator representation of $(\lambda\mathcal{I} + \mathcal{H})$ is sparse. This method naturally extends to combinations of affine transformations of the sum space where the Hilbert transform decouples across the affine transformations. By constructing a dual sum space that contains the range of the derivative of the sum space, we exploit a relationship between the sqrt-Laplacian, derivative and Hilbert transform (see (2.9)) to solve (\star) .

There exist many methods for tackling problems involving fractional Laplacian terms. Finite element methods (FEM) are popular, for instance see [9, 32] and the references therein. Typically during the construction of FEM, the boundary must be bounded. This implies that special care must be taken for the imposed boundary conditions as the different definitions of the fractional Laplacian are no longer equivalent. Moreover, the solutions themselves are often heavy-tailed, i.e. they decay at the rate of a Cauchy distribution rather than a Gaussian (see Section 6.4) [46, Sec. 2]. Hence, FEM naïvely applied to a (large) truncation of an unbounded domain will likely exhibit numerical artefacts due to the nonlocal nature of the operators [19, Sec. 9].

Spectral methods for tackling Helmholtz-like problems posed on \mathbb{R}^d can also be found in the literature [16, 31, 33, 39, 41, 42]. For a summary see [19]. Mao and Shen [33]

developed a Hermite spectral method to solve the fractional Helmholtz problem ($\lambda > 0$, $\eta = \mu = 0$) on unbounded domains, $d \in \{1, 2\}$, for an arbitrary fractional Laplacian $(-\Delta)^s$, $s \in (0, 1)$. Each solve relied on four discrete Hermite transforms. They also developed a Galerkin method where the stiffness matrix entries can be computed by explicit integrals, however, the stiffness matrix is dense. Li et al. [31] also develop a spectral-Galerkin method based on Hermite polynomials and their stiffness matrix is also dense. They are also able to define a truncated fractional Laplacian. Tang et al. [42] developed a Hermite collocation method where they derived explicit recurrence relationships for the entries in the stiffness matrix. They applied their method for $d \in \{1, 2\}$ as well as to nonlinear problems. Similarly, as they use a collocation method, their linear systems are dense. Then, Tang et al. [41] extended their collocation method to modified mapped Gegenbauer functions which are better suited to approximating solutions with algebraic decay rates. Sheng et al. [39] note that for dimensions two or more, the previous methods can become expensive. Sheng et al. developed a Chebyshev spectral Galerkin method for the fractional positive-definite Helmholtz equation on an unbounded domain using the Dunford–Taylor formulation of the fractional Laplacian [10, Thm. 4.1]. They construct so-called mapped Chebyshev functions defined on \mathbb{R} . Their method works for arbitrary $s \in (0, 1)$ and they considered one, two, and three-dimensional problems. The initialization of their algorithm requires the solution of an eigenvalue problem with worst case complexity $\mathcal{O}(n^3)$ in one dimension. However, they remark this can be improved to $\mathcal{O}(n^2)$ with an optimal solver. Each solve requires an FFT and the complexity of the solve is $\mathcal{O}(n(\log n)^d)$, where d is the dimension.

We reiterate some advantages of our method. We can handle the terms $\frac{d}{dx}$ and \mathcal{H} as well as $(-\Delta)^{1/2}$ and \mathcal{I} , the former of which are not included in the aforementioned works. Moreover, the ability to contain multiple affine transformations of the reference sum space allows one to better handle regions of discontinuity in the data resulting in better approximations. The resulting linear systems are banded and sparse. Each solve is divided into independent solves, that can be computed in parallel, involving only the functions contained in the same affine transformed sum space. This results in quick solve times. The setup requires the integral of four independent special functions per differently scaled sum space, and if all sum spaces have the same scaling (i.e. they are just translations), we require only four integrals in total. The special functions are not dependent on the right-hand side of (\star) , however, they are dependent on λ , μ , and η .

Given that the different affine transformed sum spaces have overlapping support, the fact that the operator decouples across the sum spaces seems implausible at first glance. There must be communication between the sum spaces for continuity purposes. The communication occurs during the expansion of the right-hand side: a process that cannot be decoupled across different affine transformed sum spaces. Hence, the computational

expense shifts from the solve of the equation to an interpolation of a known function [2, 3].

Remark 1.1. *As the sum spaces centred at multiple intervals are combined together to form the overall approximation space, it is tempting to call this a spectral element method. We avoid using the terminology “element” as it may be confusing. The support of a sum space function centred at an interval is not necessarily contained within the interval. In fact the support of the approximation space is always \mathbb{R} . Moreover, the expansion of the right-hand side is slightly more difficult than a typical finite/spectral element method as the sum space functions centred at different intervals all interact. However, we emphasize that the operator $L_{\lambda,\mu,\eta}$ decouples across sum space functions centred at different intervals. Hence, given an expansion of the right-hand side, the solve complexity only increases linearly with the number of intervals used and the solve over different intervals can be done in parallel.*

2 Mathematical setup

Let $W^{s,p}(\mathbb{R})$ denote the (possibly fractional) Sobolev space [1, 20] and $H^s(\mathbb{R}) := W^{s,2}(\mathbb{R})$. We denote the Lebesgue space by $L^s(\mathbb{R})$, $s > 0$. We seek a solution $u \in H^{1/2}(\mathbb{R})$ for (\star) . Moreover, if $\eta \neq 0$, then we require the stronger assumption that $u \in H^1(\mathbb{R})$. We note that $H^1(\mathbb{R}) \subset H^{1/2}(\mathbb{R})$ which follows from the (Fourier) definition of $H^1(\mathbb{R})$ [1, Sec. 7.62] and a small extension to [20, Prop. 3.6]. Similarly, the right-hand side f must have sufficient regularity so that (\star) is well-posed. Let $H^{-s}(\mathbb{R})$ denote the dual of $H^s(\mathbb{R})$, then we require $f \in H^{-1/2}(\mathbb{R})$.

\mathcal{I} denotes the identity operator and $(-\Delta)^{1/2}$ denotes the fractional sqrt-Laplacian. Its definition is somewhat subtle depending on the domain and range considered. Let \mathcal{S} denote the space of Schwartz functions. For any $s \in (0, 1)$, we define $(-\Delta)^s : \mathcal{S} \rightarrow L^2(\mathbb{R})$ as [20, Sec. 3]:

$$(-\Delta)^s u(x) := c_s \int_{\mathbb{R}} \frac{u(x) - u(y)}{|x - y|^{1+2s}} dy, \text{ for a.e. } x \in \mathbb{R}, \quad c_s := \frac{4^s \Gamma(1/2 + s)}{\pi^{1/2} |\Gamma(-s)|}. \quad (2.1)$$

Here $\int_{\mathbb{R}} \cdot$ denotes the Cauchy principal value integral [29, Ch. 2.4] and $\Gamma(\cdot)$ denotes the Gamma function. For any $u \in H^s(\mathbb{R})$ it can be shown that $(-\Delta)^{s/2} u \in L^2(\mathbb{R})$ [20, Prop. 3.6] where $(-\Delta)^{s/2}$ is defined as in (2.1) for $s \in (0, 1)$. This also holds for $s = 1$ by a small extension. Thus we consider the weak form reformulation of the fractional Laplacian $(-\Delta)^s : H^s(\mathbb{R}) \rightarrow H^{-s}(\mathbb{R})$:

$$\langle (-\Delta)^s u, v \rangle_{H^{-s}(\mathbb{R}), H^s(\mathbb{R})} = \langle (-\Delta)^{s/2} u, (-\Delta)^{s/2} v \rangle_{L^2(\mathbb{R})} \text{ for all } v \in H^s(\mathbb{R}). \quad (2.2)$$

The right-hand side of (2.2) is often referred to as the *quadratic* form of the fractional Laplacian. The quadratic form is best suited to prove existence of solutions. Suppose $\lambda > 0$ and $\eta \in \mathbb{R}$. Then the following equation has a weak solution $u_* \in H^{1/2}(\mathbb{R})$ (see Theorem 2.2),

$$\begin{aligned} \lambda \langle u, v \rangle_{L^2(\mathbb{R})} + \eta \langle \mathcal{H}u, v \rangle_{L^2(\mathbb{R})} \\ + \langle (-\Delta)^{1/4}u, (-\Delta)^{1/4}v \rangle_{L^2(\mathbb{R})} = \langle f, v \rangle_{H^{-1/2}(\mathbb{R}), H^{1/2}(\mathbb{R})}. \end{aligned} \quad (\text{W-}\star)$$

By definition of $H^{1/2}(\mathbb{R})$ we have that $u_* \in L^2(\mathbb{R})$. Moreover, if $f \in L^2(\mathbb{R})$ (and thus $(-\Delta)^{1/2}u_* \in L^2(\mathbb{R})$) then the weak solution u_* also satisfies [30, Th. 1.1]

$$(\lambda \mathcal{I} + \eta \mathcal{H} + (-\Delta)^{1/2})u_* = f \text{ a.e. in } \mathbb{R}. \quad (2.3)$$

The fractional Laplacian can also be defined via the Fourier transform. In this work we use the following conventions for the Fourier transform and its inverse, $\mathcal{F} : L^1(\mathbb{R}) \rightarrow C(\mathbb{R})$:

$$\mathcal{F}[f](\omega) = \int_{\mathbb{R}} f(x)e^{-i\omega x} dx, \quad \mathcal{F}^{-1}[F](x) = \frac{1}{2\pi} \int_{\mathbb{R}} F(\omega)e^{i\omega x} d\omega. \quad (2.4)$$

The Fourier transform is an automorphism for the space \mathcal{S} , $\mathcal{F} : \mathcal{S} \rightarrow \mathcal{S}$ [8, Cor. 9.1.8]. By duality, the Fourier transform (and its inverse) can be defined for the space of tempered distributions, $\mathcal{F} : \mathcal{S}^* \rightarrow \mathcal{S}^*$, where the space of tempered solutions \mathcal{S}^* is the dual space of \mathcal{S} [8, Sec. 9.3]. As the space of Schwartz functions is dense in $L^p(\mathbb{R})$, for $p \in [1, \infty)$, the Fourier transform can be extended to all $f \in L^p(\mathbb{R})$. However, the Fourier transform may only be a tempered distribution for $p > 2$. The Hausdorff–Young inequality implies that, for $p \in [1, 2]$, $\mathcal{F} : L^p(\mathbb{R}) \rightarrow L^q(\mathbb{R})$ where $1/p + 1/q = 1$ [38, Ch. 2.3]. In general, the Fourier transform of a function $f \in L^p(\mathbb{R}) \setminus L^1(\mathbb{R})$, $p \in (1, \infty)$, cannot be computed via the formula in (2.4) [8, Sec. 9.2].

If both $u, (-\Delta)^s u \in L^p(\mathbb{R})$ for some $p \in [1, \infty)$, then the operator $(-\Delta)^s$ can be equivalently interpreted as a Fourier multiplier, i.e. the following equation holds in the sense of distributions [30, Th. 1.1]:

$$\mathcal{F}[(-\Delta)^s[u]](\omega) = |\omega|^{2s} \mathcal{F}[u](\omega). \quad (2.5)$$

If $p \in [1, 2]$, then (2.5) holds a.e. in \mathbb{R} [30, Th. 1.1].

$\mathcal{H} : L^p(\mathbb{R}) \rightarrow L^p(\mathbb{R})$, $p \in (1, \infty)$, denotes the Hilbert transform which is a bounded linear operator. It can be defined via the following convolution:

$$\mathcal{H}[u](x) := \frac{1}{\pi} \int_{\mathbb{R}} \frac{u(y)}{x-y} dy \text{ for a.e. } x \in \mathbb{R}. \quad (2.6)$$

Equivalently, the Hilbert transform can be seen as a Fourier multiplier such that [28, Sec. 2.2]

$$\mathcal{F}[\mathcal{H}[u]](\omega) = -i \operatorname{sgn}(\omega) \mathcal{F}[u](\omega), \quad (2.7)$$

where $\operatorname{sgn}(\cdot)$ denotes the sign function. A useful property of the Hilbert transform is that it is anti-self adjoint [43, Th. 102].

Lemma 2.1 (Anti-self adjointness of the Hilbert transform). *The Hilbert transform is anti-self adjoint, i.e. for $u \in L^p(\mathbb{R})$, $v \in L^q(\mathbb{R})$ such that $1 < p, q < \infty$, $1/p + 1/q = 1$,*

$$\langle \mathcal{H}[u], v \rangle_{L^p(\mathbb{R}), L^q(\mathbb{R})} = -\langle u, \mathcal{H}[v] \rangle_{L^p(\mathbb{R}), L^q(\mathbb{R})}. \quad (2.8)$$

The Hilbert transform has found uses in aerofoil theory, crack formation, elasticity, and potential theory [29]. Of particular interest here is the connection with the sqrt-Laplacian.

Theorem 2.1. *Consider any $u \in L^2(\mathbb{R})$ such that $(-\Delta)^{1/2}u \in \mathcal{S}^*$. Then, the following equation holds in the sense of distributions:*

$$\frac{d}{dx} \mathcal{H}[u] = (-\Delta)^{1/2}[u]. \quad (2.9)$$

Proof. For any $u \in L^2(\mathbb{R})$, $(-\Delta)^{1/2}u$ is defined as follows: for any $\phi \in \mathcal{S}$ [30],

$$\int_{\mathbb{R}} (-\Delta)^{1/2}[u] \phi \, dx = \int_{\mathbb{R}} u (-\Delta)^{1/2}[\phi] \, dx, \quad (2.10)$$

where $(-\Delta)^{1/2}[\phi]$ is understood via (2.1). Similarly,

$$\int_{\mathbb{R}} \frac{d}{dx} \mathcal{H}[u] \phi \, dx = - \int_{\mathbb{R}} \mathcal{H}[u] \frac{d}{dx} \phi \, dx = \int_{\mathbb{R}} u \mathcal{H} \frac{d}{dx} \phi \, dx, \quad (2.11)$$

where the first equality is the definition of the distributional derivative and the second holds by Lemma 2.1 since $u, \frac{d}{dx} \phi \in L^2(\mathbb{R})$. It remains to show that $(-\Delta)^{1/2} \phi = \mathcal{H} \frac{d}{dx} \phi$ for any $\phi \in \mathcal{S}$. This follows by comparing Fourier coefficients.

Since $\phi \in \mathcal{S}$ then $\phi \in L^2(\mathbb{R})$ and by the singular operator definition of $(-\Delta)^{1/2}$, $(-\Delta)^{1/2} \phi \in L^2(\mathbb{R})$. Hence, by a result of Kwasnicki [30, Th. 1.1], $\mathcal{F}[(-\Delta)^{1/2} \phi](\omega) = |\omega| \mathcal{F}[\phi](\omega)$ for a.e. $\omega \in \mathbb{R}$. Moreover, since $\phi \in \mathcal{S}$, then $\frac{d}{dx} \phi \in L^2(\mathbb{R})$ which implies that $\mathcal{H}[\frac{d}{dx} \phi] \in L^2(\mathbb{R})$ and, therefore, $\mathcal{F}[\mathcal{H}[\frac{d}{dx} \phi]] \in L^2(\mathbb{R})$. In particular,

$$\mathcal{F}[\mathcal{H}[\frac{d}{dx} \phi]](\omega) = -i \operatorname{sgn}(\omega) \mathcal{F}[\frac{d}{dx} \phi](\omega) = |\omega| \mathcal{F}[\phi](\omega) \text{ for a.e. } \omega \in \mathbb{R}. \quad (2.12)$$

□

For $f \in L^2(\mathbb{R})$, the same u_* that solves (W- \star) also satisfies

$$u_*(x) = \mathcal{F}^{-1}[(\lambda - i\eta \operatorname{sgn}(\omega) + |\omega|)^{-1} \mathcal{F}[f](\omega)](x), \quad (2.13)$$

whenever the right-hand side of (2.13) is well-defined (which is not automatic). For the case where $\lambda < 0$, $\eta = 0$, there may exist *standing wave* solutions to the homogeneous equation ($f = 0$). These standing waves do not decay and thus do not live in $H^{1/2}(\mathbb{R})$. However, the Fourier transform definition does not automatically select the solution that lives in $H^{1/2}(\mathbb{R})$. Thus a solution that satisfies (2.13) might not satisfy (2.2). In Section 3.4, we encounter an example where $f \in L^1(\mathbb{R}) \setminus L^2(\mathbb{R})$ (and thus $\mathcal{F}[f]$ is well-defined) such that (2.13) has a solution and the solution does not live in $H^{1/2}(\mathbb{R})$, and thus cannot be a solution of (2.2).

Theorem 2.2 (Existence). *Suppose that $\mu \in \mathbb{R}$, $\eta = 0$, $\lambda > 0$, and $f \in H^{-1/2}(\mathbb{R})$. Then, there exists a unique weak solution $u_* \in H^{1/2}(\mathbb{R})$ that satisfies (W- \star).*

Proof. The result follows by utilizing the anti-self adjointness and continuity of \mathcal{H} (see Lemma 2.1 and [37]) as well as an application of the Lax–Milgram theorem (see [33, Sec. 2.2]). \square

3 Sum space

The goal of this section is to define the four families of functions found in Fig. 1. The first row in Fig. 1 form the primal set of functions that we approximate our solution with. The action of $(-\Delta)^{1/2}$ maps the top left and right families to the bottom left and right families of functions, respectively. The map induces a diagonal matrix. By contrast, we construct the identity map from the top left family to the bottom right, and from the top right to the bottom left. These identity mappings only have two diagonals in their induced matrices that are non-zero entries. We note that there does not exist an identity operator from top left to bottom left and top right to bottom right. This is precisely why we require both families in the top and bottom rows, rather than just one. By combining the first row of families of functions and the bottom row of families of functions, we can find the sparse map induced by $\lambda\mathcal{I} + (-\Delta)^{1/2}$. The operators \mathcal{H} and $\frac{d}{dx}$ are treated similarly. Throughout this work, we use the convention $\mathbb{N} := \{1, 2, 3, \dots\}$ and $\mathbb{N}_0 := \{0, 1, 2, 3, \dots\}$.

Consider the *sum space*:

$$S := \operatorname{span}(\{\tilde{T}_n, W_n : n \in \mathbb{N}_0\}), \quad (3.1)$$

where $W_n(x) = (1 - x^2)_+^{1/2} U_n(x)$, U_n are Chebyshev polynomials of the second kind, and $(1 - x^2)_+^{1/2} = 0$ if $|x| \geq 1$. Hence, $W_n(x)$ are *weighted* Chebyshev polynomials of the

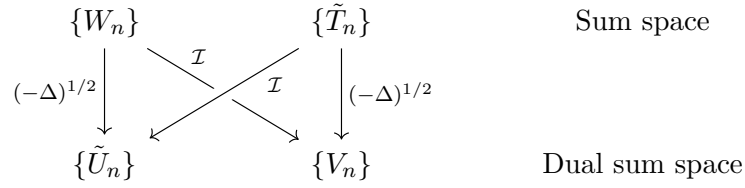


Figure 1: The domain and range of the operators $(-\Delta)^{1/2}$ and \mathcal{I} for our approximating spaces.

second kind extended to \mathbb{R} by zero. Moreover,

$$\tilde{T}_n(x) := \begin{cases} T_n(x) & \text{for } |x| \leq 1, \\ (x - \operatorname{sgn}(x)\sqrt{x^2 - 1})^n & \text{for } |x| > 1, \end{cases} \quad (3.2)$$

where $T_n(x)$ are Chebyshev polynomials of the first kind. We call $\tilde{T}_n(x)$ *extended* Chebyshev functions of the first kind. Under the change of variables, $x = \cos \theta$, for $|x| \leq 1$, the sum space is equivalent to the Fourier series on the half-period $0 \leq \theta \leq \pi$. Thus expanding a function $f(x)$ in this space is equivalent to the Fourier extension problem [11, 12, 26].

The extended Chebyshev functions \tilde{T}_n satisfy the same recurrence relationship as T_n .

Proposition 3.1 (Recurrence relation). *For all $x \in \mathbb{R}$, $n \geq 1$,*

$$2x\tilde{T}_n(x) = \tilde{T}_{n+1}(x) + \tilde{T}_{n-1}(x). \quad (3.3)$$

Proof. The case where $|x| \leq 1$ is the three-term recurrence for Chebyshev polynomials of the first kind. For $|x| > 1$, the result follows by utilizing the substitution $x = \cosh(y)$ if $x > 1$ and $x = -\cosh(y)$ if $x < -1$ into (3.3). \square

The following result is a key observation for the construction of the spectral method. The result can be found in [45, Cor. 5.7].

Proposition 3.2 (Hilbert transform). *For $x \in \mathbb{R}$, $n \in \mathbb{N}_0$, we have that*

$$\mathcal{H}[W_n](x) = \tilde{T}_{n+1}(x). \quad (3.4)$$

Moreover, for a function $u \in L^p(\mathbb{R})$, $p \in (1, \infty)$, the Hilbert transform is an anti-involution, i.e. $\mathcal{H}^2[u] = -u$. Hence,

$$\mathcal{H}[\tilde{T}_{n+1}](x) = -W_n(x). \quad (3.5)$$

Remark 3.1. *Here $\tilde{T}_0(x) = 1$ for all $x \in \mathbb{R}$. It can be shown that $\mathcal{H}[\tilde{T}_0](x) = 0$. Therefore, $\mathcal{H}^2[\tilde{T}_0](x) = 0$. This is not a contradiction as $\tilde{T}_0 \notin L^p(\mathbb{R})$ for any $p \in [1, \infty)$.*

Lemma 3.1. $W_n \in L^s(\mathbb{R}) \cap W^{1,p}(\mathbb{R})$ for $n \geq 0$, $s \in [1, \infty]$, $p \in [1, 2)$, and $\tilde{T}_n \in L^s(\mathbb{R}) \cap W^{1,p}(\mathbb{R})$ for $n \geq 1$, $s \in (1, \infty)$, $p \in (1, 2)$.

Proof. Since $W_n(x)$ are essentially bounded and supported on $[-1, 1]$, it follows immediately that $W_n \in L^p(\mathbb{R})$ for all $n \geq 0$, $p \in [1, \infty]$. A direct check reveals that $W_n \in W^{1,p}(\mathbb{R})$ for $p \in [1, 2)$. Moreover, for any function $f \in L^s(\mathbb{R})$, $s \in (1, \infty)$, we have that [37]

$$\|\mathcal{H}f\|_{L^s(\mathbb{R})} \leq C\|f\|_{L^s(\mathbb{R})}, \quad (3.6)$$

for a constant C that only depends on s . Hence, for $n \geq 1$,

$$\|\tilde{T}_n\|_{L^s(\mathbb{R})} = \|\mathcal{H}W_{n-1}\|_{L^s(\mathbb{R})} \leq C\|W_{n-1}\|_{L^s(\mathbb{R})} < \infty. \quad (3.7)$$

As $\frac{d}{dx}$ and \mathcal{H} commute for any function in $W^{1,q}(\mathbb{R})$, $q \in (1, \infty)$ [28, Th. 3.2], we have that $\mathcal{H}\frac{d}{dx}\tilde{T}_n(x) = \frac{d}{dx}W_{n-1}(x)$ a.e. Thus, for any $p \in (1, 2)$, $n \geq 1$,

$$\left\|\frac{d}{dx}\tilde{T}_n\right\|_{L^p(\mathbb{R})} = \left\|\mathcal{H}\frac{d}{dx}W_{n-1}\right\|_{L^p(\mathbb{R})} \leq C\left\|\frac{d}{dx}W_{n-1}\right\|_{L^p(\mathbb{R})} < \infty. \quad (3.8)$$

Therefore, $\tilde{T}_n \in L^s(\mathbb{R}) \cap W^{1,p}(\mathbb{R})$ for $n \geq 1$, $s \in (1, \infty)$, $p \in (1, 2)$. \square

Consider the expansion, for $x \in \mathbb{R}$,

$$u(x) = \tilde{u}_0\tilde{T}_0(x) + \sum_{n=1}^{\infty}[\tilde{u}_n\tilde{T}_n(x) + u_nW_{n-1}(x)], \quad (3.9)$$

where $\{\tilde{u}_n\}, \{u_n\} \subset \mathbb{R}$ are constants. Then, a calculation shows that, for $x \in \mathbb{R}$,

$$(\lambda\mathcal{I} + \mu\mathcal{H})[u](x) = \lambda\tilde{u}_0\tilde{T}_0(x) + \sum_{n=1}^{\infty}[(\lambda\tilde{u}_n + \mu u_n)\tilde{T}_n(x) + (\lambda u_n - \mu\tilde{u}_n)W_{n-1}(x)], \quad (3.10)$$

i.e. the $(\lambda\mathcal{I} + \mu\mathcal{H})$ operator maps the expansion to itself. Consider the equation $(\lambda\mathcal{I} + \mu\mathcal{H})[u] = f$. If one has an expansion for the right-hand side term, f , in the sum space, then it is possible to quickly compute the corresponding solution, u , via (3.10).

Remark 3.2. *We note that the Hilbert transform relationship (3.4) also holds for scaled and shifted Chebyshev polynomials. This provides the bedrock for the decoupling of the Hilbert transform problem across affine transformed sum spaces.*

We note that the sum space is a so-called *frame* for $x \in [-1, 1]$ [2].

Definition 3.1. *Consider a Hilbert space H . An indexed family of functions $\{\phi_n\} \in H$ is called a frame for H if there exist constants $0 < c \leq C < \infty$ such that*

$$c\|f\|_H^2 \leq \sum_n |\langle f, \phi_n \rangle_H|^2 \leq C\|f\|_H^2 \text{ for all } f \in H. \quad (3.11)$$

The following proposition is equivalent to a similar result by Huybrechs [26, Cor. 3.2] concerning a frame for Fourier extensions, as our space restricted to $[-1, 1]$ is equivalent to the Fourier basis functions restricted to $[-1, 1]$.

Proposition 3.3 (Frame). *Let $\beta(x) := (1 - x^2)_+^{-1/2}$ and denote the weighted Lebesgue space by $L^2_\beta(-1, 1)$ equipped with the inner product $\langle f, g \rangle_{L^2_\beta(-1, 1)} = \int_{-1}^1 fg\beta \, dx$. Then, the sum space S , for $x \in (-1, 1)$, is a frame on $L^2_\beta(-1, 1)$.*

Proof. The families of Chebyshev polynomials $T_n(x)$ and $U_n(x)$ are orthogonal with respect to the weights $(1 - x^2)_+^{-1/2}$ and $(1 - x^2)_+^{1/2}$, respectively on $L^2(-1, 1)$. Consider any $f \in L^2_\beta(-1, 1)$. By noting $\tilde{T}_n(x) = T_n(x)$ for $x \in [-1, 1]$ and two applications of Parseval's identity, we see that

$$\begin{aligned} & \sum_{n=0}^{\infty} \left[|\langle f, \tilde{T}_n \rangle_{L^2_\beta(-1, 1)}|^2 + |\langle f, W_n \rangle_{L^2_\beta(-1, 1)}|^2 \right] \\ &= \sum_{n=0}^{\infty} \left[|\langle f, \beta T_n \rangle_{L^2(-1, 1)}|^2 + |\langle f\beta, W_n \rangle_{L^2(-1, 1)}|^2 \right] \\ &= \|f\|_{L^2_\beta(-1, 1)}^2 + \|f\beta\|_{L^2_{1/\beta}(-1, 1)}^2 = 2\|f\|_{L^2_\beta(-1, 1)}^2. \end{aligned} \tag{3.12}$$

Thus the lower and upper bound constants in (3.11) are $c = C = 2$. \square

Remark 3.3. *Suppose that the support of a function is contained in the union of user-chosen intervals. Then the function can be represented to arbitrary precision by the frame induced by taking the union of all the sum space functions centred on all the affine transformed sum spaces (see Section 4 and Proposition 4.1).*

3.1 Dual sum space

In order to exploit the relationship (2.9), we require the action of the derivative on the sum space. Let $V_n(x) := (1 - x^2)_+^{-1/2}T_n(x)$, $x \in \mathbb{R}$, denote the weighted Chebyshev polynomial of the first kind of order n extended to \mathbb{R} by zero. Define, $(1 - x^2)_+^{-1/2} = 0$ if $|x| \geq 1$. Consider the following functions:

$$\tilde{U}_{-2}(x) := \begin{cases} 0 & |x| \leq 1, \\ -\frac{|x|}{\sqrt{x^2-1}} & |x| > 1, \end{cases} \quad \tilde{U}_{-1}(x) := \begin{cases} 0 & |x| \leq 1, \\ -\frac{\operatorname{sgn}(x)}{\sqrt{x^2-1}} & |x| > 1. \end{cases} \tag{3.13}$$

Furthermore, for $x \in \mathbb{R}$, we define

$$\tilde{U}_0(x) := \tilde{T}_0(x) + \tilde{U}_{-2}(x), \tag{3.14}$$

and, for $n \in \mathbb{N}$, we recursively define the extended Chebyshev functions of the second kind as follows:

$$\tilde{U}_n(x) := 2\tilde{T}_n(x) + \tilde{U}_{n-2}(x). \quad (3.15)$$

The dual sum space is given by

$$S^* := \text{span}(\{\tilde{U}_m, V_n : m \in \mathbb{N}_0 \cup \{-2, -1\}, n \in \mathbb{N}_0\}). \quad (3.16)$$

The weighted Chebyshev polynomials and extended Chebyshev functions have been centred on the interval $[-1, 1]$.

Definition 3.2 (Affine transformation). *Consider an interval $I = [a, b] \subset \mathbb{R}$, $a < b$ and the affine transformation $y = 2/(b-a)(x - (a+b)/2)$. We define the affine transformed extended and weighted Chebyshev functions and polynomials, centred at I , as $\tilde{T}_n^I(x) = \tilde{T}_n(y)$, $\tilde{U}_n^I(x) = \tilde{U}_n(y)$, $W_n^I(x) = W_n(y)$, and $V_n^I(x) = V_n(y)$.*

We note that $W_n^I(x)$ and $V_n^I(x)$ are supported on the interval I , whereas $\tilde{T}_n^I(x)$ and $\tilde{U}_n^I(x)$ have global support extending beyond I .

In the following proposition we show some relationships between the sum space and the dual sum space.

Proposition 3.4 (Equality and derivatives). *Consider the interval $I = [a, b] \subset \mathbb{R}$, $a < b$. Then, for any $n \in \mathbb{N}$, $x \in \mathbb{R} \setminus \{a, b\}$,*

$$\frac{d}{dx} \tilde{T}_n^I(x) = \frac{2n}{b-a} \tilde{U}_{n-1}^I(x), \quad (3.17)$$

and, for $n \in \mathbb{N}_0$,

$$\frac{d}{dx} W_n^I(x) = -\frac{2(n+1)}{b-a} V_{n+1}^I(x). \quad (3.18)$$

Moreover, for any $x \in \mathbb{R}$,

$$W_n^I(x) = \frac{1}{2}[V_n^I(x) - V_{n+2}^I(x)]. \quad (3.19)$$

Proof. All three identities (3.17)–(3.19) follow from classical identities between Chebyshev polynomials of the first and second kinds, their recurrence relationships, and an induction argument. We prove the first identity (3.17) and note that the other two are found in the literature [36, Sec. 18.9.10 & 18.9.22].

We consider (3.17) and initially examine the case where $I = [-1, 1]$. Consider the region $x \in [-1, 1]$. From the definition of $\tilde{U}_n(x)$, for $n \geq 0$, in (3.14) and (3.15), and

a classical identity between Chebyshev polynomials of the first and second kinds [36, Sec. 18.9.9], it can be shown that

$$\tilde{U}_n(x) = U_n(x), \quad n \geq 0, \quad \text{for } x \in [-1, 1], \quad (3.20)$$

where $U_n(x)$ are the Chebyshev polynomials of the second kind. Hence, another classical identity [36, Sec. 18.9.21] reveals that

$$\frac{d}{dx} \tilde{T}_n(x) = n \tilde{U}_{n-1}(x) \quad \text{for } x \in (-1, 1). \quad (3.21)$$

Consider $|x| > 1$. By a direct calculation we see that

$$\frac{d}{dx} \tilde{T}_1(x) = \tilde{U}_0(x) \quad \text{and} \quad \frac{d}{dx} \tilde{T}_2(x) = 2\tilde{U}_1(x). \quad (3.22)$$

Moreover, another direct calculation shows that, for $|x| > 1$ and $n \geq 2$,

$$\frac{d}{dx} \tilde{T}_n(x) = -\operatorname{sgn}(x) \frac{n(x - \operatorname{sgn}(x)\sqrt{x^2 - 1})^n}{\sqrt{x^2 - 1}}. \quad (3.23)$$

Suppose that (3.17) holds up to and including $\tilde{T}_{n-1}(x)$. Now,

$$n\tilde{U}_{n-1}(x) = 2n\tilde{T}_{n-1}(x) + n\tilde{U}_{n-3}(x) = 2n\tilde{T}_{n-1}(x) + \frac{n}{n-2} \frac{d}{dx} \tilde{T}_{n-2}(x), \quad (3.24)$$

where the first equality follows by definition of $\tilde{U}_n(x)$ and the second equality follows from the induction argument. Substituting in the explicit definitions of $\tilde{T}_{n-1}(x)$ and $\frac{d}{dx} \tilde{T}_{n-2}(x)$, $|x| > 1$, we find that the right-hand side of (3.24) is equal to (3.21). Hence, (3.17) holds for all $n \in \mathbb{N}$, $x \in \mathbb{R} \setminus \{-1, 1\}$, when $I = [-1, 1]$, by induction. It follows by applying the chain rule that (3.17) holds for arbitrary $I = [a, b]$. \square

Proposition 3.5 (Sqrt-Laplacian). *Consider the interval $I = [a, b] \subset \mathbb{R}$, $a < b$. Then, for any $n \in \mathbb{N}$, $x \in \mathbb{R} \setminus \{a, b\}$,*

$$(-\Delta)^{1/2}[\tilde{T}_n^I](x) = \frac{2n}{b-a} V_n^I(x), \quad (3.25)$$

and, for $n \in \mathbb{N}_0$, $x \in \mathbb{R} \setminus \{a, b\}$,

$$(-\Delta)^{1/2}[W_n^I](x) = \frac{2(n+1)}{b-a} \tilde{U}_n^I(x). \quad (3.26)$$

Proof. By Lemma 3.1, $\tilde{T}_n, W_m \in L^2(\mathbb{R}) \cap W^{1,s}(\mathbb{R})$, $s \in (1, 2)$, $n \geq 1$, $m \geq 0$. Thus the conditions of Theorem 2.1 hold and $(-\Delta)^{1/2}[\tilde{T}_n] = \frac{d}{dx} \mathcal{H}[\tilde{T}_n]$ and $(-\Delta)^{1/2}[W_m] = \frac{d}{dx} \mathcal{H}[W_m]$ in the sense of distributions. The result then follows by applying Proposition 3.2 and Proposition 3.4. \square

Corollary 3.1 (Hilbert transforms of V_n^I and \tilde{U}_n^I). *Consider the interval $I = [a, b] \subset \mathbb{R}$, $a < b$. Then, for $n \geq 0$,*

$$\mathcal{H}[\tilde{U}_n^I](x) = V_{n+1}^I(x) \text{ and } \mathcal{H}[V_{n+1}^I](x) = -\tilde{U}_n^I(x). \quad (3.27)$$

Proof. We note that

$$\mathcal{H}[\tilde{U}_n^I] = \mathcal{H} \frac{d}{dx} \left[\frac{b-a}{2(n+1)} \tilde{T}_{n+1}^I \right] = -\frac{d}{dx} \frac{b-a}{2(n+1)} W_n^I = V_{n+1}^I, \quad (3.28)$$

where the first and third equalities follow from Proposition 3.4 and the second equality holds as $\tilde{T}_{n+1}^I \in W^{1,p}(\mathbb{R})$ for any $p \in (1, 2)$ [28, Th. 3.2]. The second result follows as \mathcal{H} is an anti-involution. \square

Corollary 3.2 (Regularity of $(-\Delta)^{1/2} \tilde{T}_n^I$ and $(-\Delta)^{1/2} W_n^I$). *Consider the interval $I = [a, b] \subset \mathbb{R}$, $a < b$. Then, $(-\Delta)^{1/2} \tilde{T}_n^I, (-\Delta)^{1/2} W_m^I \in L^p(\mathbb{R})$ for any $p \in (1, 2)$, $n \in \mathbb{N}$, $m \in \mathbb{N}_0$.*

Proof. A direct check reveals that $V_m^I(x) \in L^p(\mathbb{R})$ for any $p \in [1, 2)$, $m \in \mathbb{N}_0$. Hence, by Proposition 3.5, $(-\Delta)^{1/2} \tilde{T}_m^I \in L^p(\mathbb{R})$ for any $p \in (1, 2)$. Moreover, for any $p \in (1, 2)$,

$$\begin{aligned} \|(-\Delta)^{1/2} W_n^I\|_{L^p(\mathbb{R})} &= \frac{2(n+1)}{b-a} \|\tilde{U}_n^I\|_{L^p(\mathbb{R})} \\ &= \frac{2(n+1)}{b-a} \|\mathcal{H}V_{n+1}^I\|_{L^p(\mathbb{R})} \leq \frac{2C(n+1)}{b-a} \|V_{n+1}^I\|_{L^p(\mathbb{R})} < \infty. \end{aligned} \quad (3.29)$$

\square

The Hilbert space $H^{1/2}(\mathbb{R})$ is equipped with the inner-product

$$\langle u, v \rangle_{H^{1/2}(\mathbb{R})} := \langle u, v \rangle_{L^2(\mathbb{R})} + \langle (-\Delta)^{1/4} u, (-\Delta)^{1/4} v \rangle_{L^2(\mathbb{R})}. \quad (3.30)$$

The following proposition shows that $\tilde{T}_n(x)$ and W_n have partial orthogonality with respect to the $H^{1/2}(\mathbb{R})$ inner product.

Proposition 3.6 (Partial orthogonality in $H^{1/2}(\mathbb{R})$). *$\tilde{T}_n, W_m, n \in \mathbb{N}, m \in \mathbb{N}_0$ satisfy*

$$\langle (-\Delta)^{1/4} \tilde{T}_j, (-\Delta)^{1/4} \tilde{T}_l \rangle_{L^2(\mathbb{R})} = l \delta_{jl}, \quad \langle (-\Delta)^{1/4} W_j, (-\Delta)^{1/4} W_l \rangle_{L^2(\mathbb{R})} = (l+1) \delta_{jl}, \quad (3.31)$$

where δ_{jl} is the Kronecker delta.

Proof. We note that

$$\begin{aligned} \langle (-\Delta)^{1/4} \tilde{T}_j, (-\Delta)^{1/4} \tilde{T}_l \rangle_{L^2(\mathbb{R})} &= \langle \tilde{T}_j, (-\Delta)^{1/2} \tilde{T}_l \rangle_{L^2(\mathbb{R})} = l \langle \tilde{T}_j, V_l \rangle_{L^2(\mathbb{R})} \\ &= l \langle T_j, V_l \rangle_{L^2(-1,1)} = l \delta_{jl}. \end{aligned} \quad (3.32)$$

Similarly,

$$\begin{aligned} \langle (-\Delta)^{1/4} W_j, (-\Delta)^{1/4} W_l \rangle_{L^2(\mathbb{R})} &= \langle W_j, (-\Delta)^{1/2} W_l \rangle_{L^2(\mathbb{R})} = (l+1) \langle W_j, \tilde{U}_l \rangle_{L^2(\mathbb{R})} \\ &= (l+1) \langle W_j, U_l \rangle_{L^2(-1,1)} = (l+1) \delta_{jl}. \end{aligned} \quad (3.33)$$

\square

3.2 Operators

For any $x \in \mathbb{R}$, we denote the n -th sum space and dual sum space quasimatrices, centred at an interval $I = [a, b] \subset \mathbb{R}$, by

$$S_n^I(x) := \left(\tilde{T}_0^I(x) \mid W_0^I(x) \quad \tilde{T}_1^I(x) \mid \cdots \mid W_n^I(x) \quad \tilde{T}_{n+1}^I(x) \right), \quad (3.34)$$

$$S_n^{I,*}(x) := \left(\tilde{U}_{-2}^I(x) \mid V_0^I(x) \quad \tilde{U}_{-1}^I(x) \mid \cdots \mid V_{n+2}^I(x) \quad \tilde{U}_{n+1}^I(x) \right). \quad (3.35)$$

A quasimatrix is a matrix whose ‘‘columns’’ are functions defined on \mathbb{R} [40, Lec. 5]. In $S_n^I(x)$ the first column contains the constant function. Thereafter, we block together the columns $W_k^I(x)$ and $\tilde{T}_{k+1}^I(x)$ for $k = 0, \dots, n$. Similarly in $S_n^{I,*}(x)$, the first column contains $\tilde{U}_{-2}^I(x)$. Thereafter, we block together the columns $V_k^I(x)$ and $\tilde{U}_{k-1}^I(x)$ for $k = 0, \dots, n+2$. We note that $S_n^{I,*}(x)$ has four more columns than $S_n^I(x)$. These are required to represent the identity map between the two sum spaces exactly.

Proposition 3.7 (Quasimatrix operators). *Consider the interval $I = [a, b] \subset \mathbb{R}$, $a < b$. Then, for $x \in \mathbb{R}$,*

$$S_n^I(x) = S_n^{I,*}(x)E, \quad \mathcal{H}[S_n^I](x) = S_n^{I,*}(x)H, \quad (3.36)$$

and for $x \in \mathbb{R} \setminus \{a, b\}$,

$$\frac{d}{dx}[S_n^I](x) = S_n^{I,*}(x)D^I, \quad \text{and } (-\Delta)^{1/2}[S_n^I](x) = S_n^{I,*}(x)A^I. \quad (3.37)$$

Let

$$N = \begin{pmatrix} -1 & 0 \\ 0 & 1 \end{pmatrix}, \quad M = \begin{pmatrix} 0 & 1 \\ 1 & 0 \end{pmatrix}, \quad Z = \begin{pmatrix} 0 & 0 \\ 0 & 0 \end{pmatrix}, \quad \mathbf{0} = \begin{pmatrix} 0 \\ 0 \end{pmatrix}, \quad \mathbf{e}_2 = \begin{pmatrix} 0 \\ 1 \end{pmatrix}. \quad (3.38)$$

Then $E, H, D^I, A^I \in \mathbb{R}^{(2n+7) \times (2n+3)}$ are defined by

$$E := \begin{pmatrix} -1 & \mathbf{0}^\top & \dots & & \\ \mathbf{0} & -N/2 & & & \\ \mathbf{e}_2 & Z & \ddots & & \\ \mathbf{0} & N/2 & \ddots & -N/2 & \\ \vdots & & \ddots & Z & \\ & & & & N/2 \end{pmatrix}, \quad (3.39)$$

$$H := \begin{pmatrix} 0 & \dots & & & \\ \vdots & -M/2 & & & \\ & Z & \ddots & & \\ & M/2 & \ddots & -M/2 & \\ & & \ddots & Z & \\ & & & & M/2 \end{pmatrix}, \quad (3.40)$$

$$D^I := \begin{pmatrix} 0 & \dots & & & \\ \vdots & Z & & & \\ & \frac{2}{b-a}N & & & \\ & & \frac{4}{b-a}N & & \\ & & & \ddots & \\ & & & & \frac{2(n+1)}{b-a}N \\ & & & & Z \end{pmatrix}, \quad (3.41)$$

$$A^I := \begin{pmatrix} 0 & \dots & & & \\ \vdots & Z & & & \\ & \frac{2}{b-a}M & & & \\ & & \frac{4}{b-a}M & & \\ & & & \ddots & \\ & & & & \frac{2(n+1)}{b-a}M \\ & & & & Z \end{pmatrix}. \quad (3.42)$$

Proof. The result follows from Propositions 3.2, 3.4, and 3.5. \square

Proposition 3.8 (Jacobi matrix). *Consider the interval $I = [a, b] \subset \mathbb{R}$, $a < b$. Let S_∞^I denote the quasimatrix of the entire sum space, i.e. S_n^I with $n = \infty$. Moreover, let $S_\infty^{\circ I}$ denote S_∞^I but with the first column (\tilde{T}_0) removed. For any $x \in \mathbb{R}$, let $y =$*

$2/(b-a)(x - (a+b)/2)$. Then,

$$yS_\infty^{\circ,I}(x) = S_\infty^I(x)J \quad (3.43)$$

where

$$J := \begin{pmatrix} 0 & 1/2 & 0 & & \\ 0 & 0 & 1/2 & & \\ 0 & 0 & 0 & \ddots & \\ 1/2 & 0 & 0 & & \\ 0 & 1/2 & 0 & & \\ & & & \ddots & \end{pmatrix}. \quad (3.44)$$

Proof. The Jacobi matrix of W_n is the same as the Jacobi matrix for U_n . The entries of the columns associated with \tilde{T}_n follow from Proposition 3.1. \square

Remark 3.4. The matrices E , H , D^I , A^I , and J are sparse.

3.3 Single interval

We now collect the final ingredients for the spectral method centred on a single interval at $[-1, 1]$ to solve (\star) for $x \in \mathbb{R}$. Consider the expansion of the right-hand side $f(x)$ in the dual sum space and truncate at degree n ,

$$f(x) \approx S_n^*(x)\mathbf{f}, \quad \mathbf{f} \in \mathbb{R}^{2n+7}. \quad (3.45)$$

Consider the matrix $L := \lambda E + \mu H + \eta D^I + A^I$. We note that L is a linear operator mapping from the sum space $S_n(x)$ to the dual sum space $S_n^*(x)$. However, $L \in \mathbb{R}^{(2n+7) \times (2n+3)}$ is a rectangular matrix and the linear system

$$L\mathbf{u} = \mathbf{f}, \quad (3.46)$$

to find the coefficients of $u(x)$ in the truncated sum space is overdetermined. We wish to construct a method where the expansion of $u(x)$ is determined exactly i.e. we want to avoid a least squares solution for \mathbf{u} . Let $S_n^\circ(x)$ denote the sum space $S_n(x)$ without the first block, i.e. we drop the first function $\tilde{T}_0(x)$. We construct the following *appended sum space*

$$S_n^+(x) := \left(\tilde{T}_0(x) \mid v_0(x) \quad \tilde{u}_{-1}(x) \mid v_1(x) \quad \tilde{u}_0(x) \mid S_n^\circ(x) \right). \quad (3.47)$$

Here, the functions $v_n(x)$ and $\tilde{u}_n(x)$ satisfy

$$\mathcal{L}_{\lambda,\mu,\eta}\tilde{u}_n(x) = \tilde{U}_n(x), \quad (3.48)$$

$$\mathcal{L}_{\lambda,\mu,\eta}v_n(x) = V_n(x). \quad (3.49)$$

Let $L^\circ \in \mathbb{R}^{(2n+7) \times (2n+2)}$ denote the matrix L without the first column. By considering the map induced by $L_{\lambda, \mu, \eta}$ from the appended sum space $S_n^+(x)$ to the dual sum space $S_n^*(x)$, we see that the solution of (\star) can be approximated by solving

$$L^+ \mathbf{u}^+ = \mathbf{f}, \quad (3.50)$$

where $L^+ \in \mathbb{R}^{(2n+7) \times (2n+7)}$ is the following square matrix:

$$L^+ := \left(\begin{array}{ccccc|c} -\lambda & 0 & 0 & 0 & 0 & \\ 0 & 1 & 0 & 0 & 0 & \\ 0 & 0 & 1 & 0 & 0 & \\ 0 & 0 & 0 & 1 & 0 & \\ \lambda & 0 & 0 & 0 & 1 & \\ 0 & 0 & 0 & 0 & 0 & \\ \vdots & \vdots & \vdots & \vdots & \vdots & \\ 0 & 0 & 0 & 0 & 0 & \end{array} L^\circ \right). \quad (3.51)$$

L^+ is constructed by pre-appending L with four columns containing one nonzero entry each and commuting the column associated with $\tilde{T}_0(x)$ to be first. The entries in the new columns have a value of 1 and are in the positions $(2, 2)$, $(3, 3)$, $(4, 4)$, $(5, 5)$. By solving the linear system (3.50), we conclude that $u(x) \approx S_n^+(x) \mathbf{u}^+$. In order to realize the values of $S_n^+(x) \mathbf{u}^+$, we require approximations for the solutions in equations (3.48) and (3.49). These can be found using a fast Fourier transform (FFT) [17], specialized quadrature formulas or explicit expressions. We give more details below.

Remark 3.5. *The solutions $\tilde{u}_n(x)$ and $v_n(x)$ are not dependent on the right-hand side f of (\star) , although they are dependent on the constants λ , μ , and η .*

Remark 3.6. *The choice of $v_0(x)$, $\tilde{u}_{-1}(x)$, $v_1(x)$ and $\tilde{u}_0(x)$ as the additional functions is not the only option. Indeed, if the goal was to improve the conditioning of L^+ , then a better choice would be $\tilde{u}_{n+1}(x)$ and $v_{n+2}(x)$ rather than $\tilde{u}_0(x)$ and $v_1(x)$. In this case, the conditioning of L^+ would be robust for large parameter ranges of λ , μ and η . With the presented choice, the conditioning degrades if both $\mu \rightarrow 0$ and $\lambda \rightarrow 0$. The disadvantage of $\tilde{u}_{n+1}(x)$ and $v_{n+2}(x)$ is that if multiple solves are required with different degrees n , then additional work is required to compute the required additional functions. Furthermore, in numerical experiments, we observed that the approximate identity mapping from the appended sum space $S_n^+(x)$ to the dual sum space $S_n^*(x)$ is unstable when using $\tilde{u}_{n+1}(x)$ and $v_{n+2}(x)$ as the additional functions. Hence, for discretized time-dependent problems where we are required to map the current solution iterate expanded in the appended sum space to the expansion in the dual sum space (for the right-hand side), this poses a distinct issue. The choice of the additional functions is context dependent.*

Proposition 3.9 (Fourier transforms of $V_n(x)$). *The weighted Chebyshev polynomials, $V_n(x)$, $n \geq 0$, have the Fourier transforms*

$$\mathcal{F}[V_n](\omega) = (-i)^n \pi J_n(\omega), \quad (3.52)$$

where J_n , $n \in \mathbb{N}_0$, denote the Bessel functions of the first kind [36, Sec. 10.2].

Proof. This is a known result and follows from an application of Parseval's integral and recurrence relationships between Bessel functions [47, Ch. 13]. \square

The following result follows by a direct calculation.

Proposition 3.10 (Fourier transforms of $\tilde{U}_n(x)$). *The extended Chebyshev functions $\tilde{U}_{-1}(x)$, $\tilde{U}_0(x)$ have the following Fourier transforms,*

$$\mathcal{F}[\tilde{U}_{-1}](\omega) = \frac{i\omega\pi J_0(\omega)}{|\omega|}, \quad \mathcal{F}[\tilde{U}_0](\omega) = \pi J_1(|\omega|) + \frac{2\sin(\omega)}{\omega} - \frac{2\sin(|\omega|)}{|\omega|}. \quad (3.53)$$

By taking the Fourier transform on both sides in (3.48) and (3.49), utilizing Propositions 3.9 and 3.10 as well as (2.5), (2.7), and $\mathcal{F}[\frac{d}{dx}u](\omega) = i\omega\mathcal{F}[u](\omega)$, we observe that

$$\mathcal{F}[\tilde{u}_{-1}](\omega) = i\pi(\lambda - i\mu \operatorname{sgn}(\omega) + i\eta\omega + |\omega|)^{-1} |\omega|^{-1} \omega J_0(\omega), \quad (3.54)$$

$$\mathcal{F}[\tilde{u}_0](\omega) = (\lambda - i\mu \operatorname{sgn}(\omega) + i\eta\omega + |\omega|)^{-1} \left(\pi J_1(|\omega|) + \frac{2\sin(\omega)}{\omega} - \frac{2\sin(|\omega|)}{|\omega|} \right), \quad (3.55)$$

$$\mathcal{F}[v_n](\omega) = (-i)^n \pi (\lambda - i\mu \operatorname{sgn}(\omega) + i\eta\omega + |\omega|)^{-1} J_n(\omega). \quad (3.56)$$

The inverse Fourier transform to compute the solutions $\tilde{u}_{-1}(x)$, $\tilde{u}_0(x)$, $v_0(x)$ and $v_1(x)$ can be approximated via specialized quadrature rules, an FFT, or explicit expressions for certain ranges of x . The FFT is discussed in more detail in Appendix A.

We do not have exact expressions for the Fourier transforms of $\tilde{U}_n(x)$ for $n \geq 1$. However, this can be overcome by first applying a Hilbert transform to the equations in (3.48) to obtain, for $n \geq -1$,

$$\left(\lambda \mathcal{H} - \mu \mathcal{I} + \eta(-\Delta)^{1/2} - \frac{d}{dx} \right) [\tilde{u}_n](x) = \mathcal{H}[\tilde{U}_n](x) = V_{n+1}(x). \quad (3.57)$$

By taking the Fourier transform of (3.57), we find that

$$\mathcal{F}[\tilde{u}_n](\omega) = (-i)^{n+1} \pi (-i\lambda \operatorname{sgn}(\omega) - \mu + \eta|\omega| - i\omega)^{-1} J_{n+1}(\omega). \quad (3.58)$$

In the next subsections we discuss edge cases of (\star) and how they are treated in our numerical method. When $\lambda = \mu = 0$ and $\eta \in \mathbb{R}$, the additional functions are no longer

required and their associated columns (and related rows) are removed from (3.51). In particular the columns associated with $\tilde{T}_0(x)$, $v_0(x)$, $\tilde{u}_{-1}(x)$, $v_1(x)$, and $\tilde{u}_0(x)$, and the rows associated with $\tilde{U}_{-2}(x)$, $V_0(x)$, $\tilde{U}_{-1}(x)$, $V_{n+2}(x)$, and $\tilde{U}_{n+1}(x)$ are removed reducing L^+ from a $(2n+7) \times (2n+7)$ matrix to a $(2n+2) \times (2n+2)$ matrix. The exact mappings are still conserved. When $\lambda = 0$ but $|\mu| > 0$ and $\eta \in \mathbb{R}$, we keep the additional functions, although we advise using the additional functions $v_{n+2}(x)$ and $\tilde{u}_{n+1}(x)$ instead of $v_1(x)$ and $\tilde{u}_0(x)$ to alleviate ill-conditioning.

3.4 Special case of $\lambda = 0$

In this subsection we discuss the conditioning of L^+ for choices of μ and η when $\lambda = 0$. The ill-conditioning is alleviated by removing the rows of L^+ associated with functions that are no longer in the range of $\mathcal{L}_{0,\mu,\eta}S_n^+$.

3.4.1 $\lambda = \mu = \eta = 0$

The first special case that we consider is $\lambda = \mu = \eta = 0$. Here, (\star) reduces to finding $u \in H^{1/2}(\mathbb{R})$ that satisfies

$$(-\Delta)^{1/2}[u] = f. \quad (3.59)$$

The first issue is that the matrix L^+ , as constructed in (3.51), is singular. This is due to three rows and one column whose entries are all zero. The three rows correspond to the dual sum space functions $\tilde{U}_{-2}(x)$, $\tilde{U}_{n+1}(x)$, and $V_{n+2}(x)$ which do not lie in the range of $(-\Delta)^{1/2}S_n^+(x)$. The column corresponds to the sum space function $\tilde{T}_0(x)$. Hence, we remove these rows and column from L^+ resulting in an $(2n+4) \times (2n+6)$ matrix. The second issue is that the additional functions computed to form the square matrix L^+ become problematic or redundant. By Proposition 3.5, we have that $\tilde{u}_j(x) = W_j(x)$, $j \geq 0$ and $v_j(x) = \tilde{T}_j(x)$, $j \geq 1$. Hence, two of the additional functions are already included in the sum space and correspond to two columns that should be removed. At first glance, this is advantageous as this reduces L^+ to a $(2n+4) \times (2n+4)$ matrix. However, computing the remaining additional functions $\tilde{u}_{-1}(x)$ and $v_0(x)$ poses a numerical difficulty. Although $\tilde{U}_{-1}, V_0 \in H^{-1/2}(\mathbb{R})$, since $\lambda = 0$, the Lax–Milgram theorem does not guarantee existence of solutions. Attempting to compute these two solutions by a forward and inverse Fourier transform fails. Hence, as discussed in Section 1, there exist solutions that satisfy the Fourier multiplier reformulation (2.13) but not (W- \star). Ignoring these technical issues and naïvely computing the inverse Fourier

transform via (2.4) does recover the non-decaying solutions:

$$\tilde{u}_{-1}(x) = \begin{cases} -\arcsin(x) & |x| < 1, \\ -\operatorname{sgn}(x)\pi/2 & |x| \geq 1, \end{cases} \quad (3.60)$$

$$v_0(x) = \begin{cases} \log(2) - \gamma & |x| < 1, \\ \log(2) - \gamma - \operatorname{arcsinh}(\sqrt{x^2 - 1}) & |x| \geq 1. \end{cases} \quad (3.61)$$

However, as neither of these tend to zero as $|x| \rightarrow \infty$, they cannot live in $H^{1/2}(\mathbb{R})$. Therefore, we choose to remove the columns associated with $\tilde{u}_{-1}(x)$ and $v_0(x)$ as well. Since all the additional functions have been removed, we are only required to consider the range of $(-\Delta)^{1/2}S_n(x)$. The range does not include $\tilde{U}_{-1}(x)$ and $V_0(x)$. Hence, these functions can be removed from the dual sum space (whilst still preserving the exact map $(-\Delta)^{1/2} : S_n \rightarrow S_n^*$) and their corresponding rows from L^+ . In summary, we remove the columns associated with $\tilde{T}_0(x)$, $v_0(x)$, $\tilde{u}_{-1}(x)$, $v_1(x)$, and $\tilde{u}_0(x)$, and the rows associated with $\tilde{U}_{-2}(x)$, $V_0(x)$, $\tilde{U}_{-1}(x)$, $V_{n+2}(x)$, and $\tilde{U}_{n+1}(x)$ reducing L^+ from a $(2n+7) \times (2n+7)$ matrix to a $(2n+2) \times (2n+2)$ matrix. We emphasize that the action of $(-\Delta)^{1/2}$ on $S_n(x)$ is still represented exactly by the reduced L^+ .

3.4.2 $\lambda = \mu = 0$, $|\eta| > 0$

We now consider where $\lambda = \mu = 0$ but $|\eta| > 0$. This corresponds to finding $u \in H^1(\mathbb{R})$ that satisfies

$$\left(\eta \frac{d}{dx} + (-\Delta)^{1/2} \right) [u] = f.$$

This special case is similar to the previous one. Again L^+ is singular due to three rows and a column which contain only zeroes. The rows are associated with the dual sum space functions $\tilde{U}_{-2}(x)$, $\tilde{U}_{n+1}(x)$, and $V_{n+2}(x)$ which do not lie in the range of $(\eta \frac{d}{dx} + (-\Delta)^{1/2})S_n^+(x)$ and the column corresponds to $\tilde{T}_0(x)$. Hence, we remove those three rows and column. Moreover, $\tilde{u}_1(x)$ and $v_0(x)$ cannot be computed via a forward and inverse Fourier transform due to the same issues as in the previous case. Hence, the columns associated with $\tilde{u}_1(x)$ and $v_0(x)$ must also be removed. This implies that the rows associated with $V_0(x)$ and $\tilde{U}_{-1}(x)$ are now all zero and must also be removed. Hence, as in the previous case, we remove the columns associated with $\tilde{T}_0(x)$, $v_0(x)$, $\tilde{u}_{-1}(x)$, $v_1(x)$, and $\tilde{u}_0(x)$, and the rows associated with $\tilde{U}_{-2}(x)$, $V_0(x)$, $\tilde{U}_{-1}(x)$, $V_{n+2}(x)$, and $\tilde{U}_{n+1}(x)$ reducing L^+ from a $(2n+7) \times (2n+7)$ matrix to a $(2n+2) \times (2n+2)$ matrix. Moreover, the action of $(\frac{d}{dx} + (-\Delta)^{-1/2})$ on $S_n(x)$ is still represented exactly by the reduced L^+ .

Remark 3.7. *Since we have removed the additional functions from the appended sum space, the setup cost is minimal when $\lambda = \mu = 0$ and $\eta \in \mathbb{R}$ as no integrals are required.*

3.4.3 $\lambda = 0, |\mu| > 0, \eta \in \mathbb{R}$

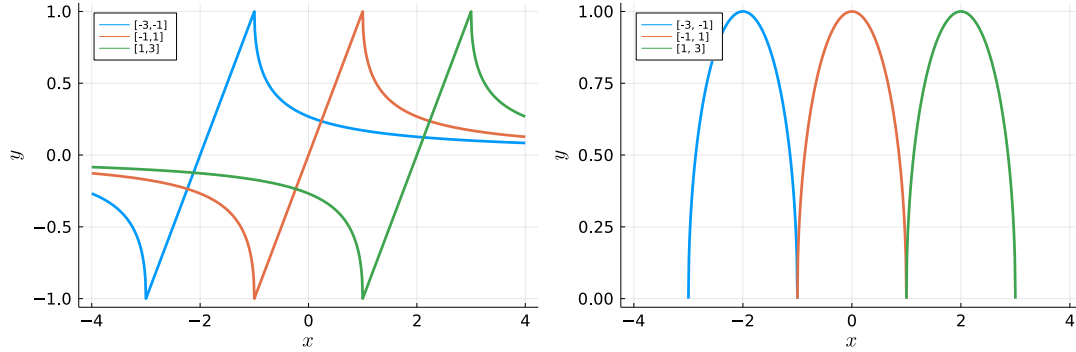
The final case to consider is when $\lambda = 0$ but $\mu \neq 0$. In this case there is only one zero row and column associated with $\tilde{U}_{-2}(x)$ and $\tilde{T}_0(x)$, respectively. Removing that row and column results in an invertible matrix that still represents the mapping exactly. Moreover, unlike the previous two cases, we recover $v_0(x), \tilde{u}_{-1}(x) \in H^{1/2}(\mathbb{R})$. However, we note that with increasing n (truncation degree) L^+ has two singular values that quickly decrease to zero which impact the conditioning of L^+ . If the problem setup requires high truncation degree n , and small parameter $|\mu| \ll 1$, then L^+ may become numerically singular. In this case, we suggest using the additional functions $v_{n+2}(x)$ and $\tilde{u}_{n+1}(x)$ instead of $v_1(x)$ and $\tilde{u}_0(x)$ as suggested in Remark 3.6. This results in a well-conditioned L^+ irrespective of the choices of n and μ .

4 Multiple intervals

Although the sum space is dense on the interval it is centred on, it is not dense in \mathbb{R} and, therefore, cannot approximate general solutions. Moreover, in some applications, it can be helpful to decompose the domain into multiple intervals. This can be in regions where (spatially varying) coefficients or right-hand sides f have discontinuities best accounted for by approximating them with sum spaces centred over two or more intervals. Experimentally, we also found that the tails of a function f outside the intervals were better approximated when using the combination of sum spaces centred at multiple intervals. Examples of low-order multiple-interval sum space functions are given in Fig. 2.

In this section, we will discuss how to combine sum spaces centred at multiple intervals together. We will show that the operator $\mathcal{L}_{\mu,\lambda,\eta}$ decouples across the different affine transformed sum spaces and this results in a linear system with a block diagonal matrix. Hence, each block can be solved separately resulting in a highly parallelizable method.

We fix the closed and bounded intervals $I_k = [a_k, b_k]$, $k = 1, \dots, K$, which may be connected but not overlap (except at a point). Consider a truncation of the expansion



(a) $\tilde{T}_1(x)$ centred at $[-3, -1]$, $[-1, 1]$ and $[1, 3]$. (b) $W_0(x)$ centred at $[-3, -1]$, $[-1, 1]$ and $[1, 3]$.

Figure 2: Plots of $\tilde{T}_1(x)$ and $W_0(x)$ centred at the three different intervals $[-3, -1]$, $[-1, 1]$ and $[1, 3]$. We note that $\tilde{T}_1(x)$ has global support and those centred on different intervals always overlap. Whereas, $W_0(x)$ has compact support on the interval it is centred on.

of a function, $g(x)$, $x \in \mathbb{R}$, in the appended multiple-interval sum space:

$$\begin{aligned}
g(x) &\approx \tilde{c}_0 \tilde{T}_0(x) \\
&+ \sum_{k=1}^K \left(c_{v_0^{I_k}} v_0^{I_k}(x) + c_{\tilde{u}_{-1}^{I_k}} \tilde{u}_{-1}^{I_k}(x) + c_{v_1^{I_k}} v_1^{I_k}(x) + c_{\tilde{u}_0^{I_k}} \tilde{u}_0^{I_k}(x) \right. \\
&\quad \left. + \sum_{j=1}^{n_k} [\tilde{c}_j^{I_k} \tilde{T}_j^{I_k}(x) + c_j^{I_k} W_{j-1}^{I_k}(x)] \right). \tag{4.1}
\end{aligned}$$

Let $S_n^{\circ, I_k, +}(x)$ denote the appended sum space centred on the interval I_k not including the constant term $\tilde{T}_0^{I_k}(x)$. Let $\mathbf{n} = (n_1, \dots, n_K)$, $N = \sum_{k=1}^K n_k$, and $\mathbf{I} = (I_1, \dots, I_K)$. Then, in quasimatrix notation, (4.1) can be rewritten as $g(x) \approx \mathbf{S}_{\mathbf{n}}^{\mathbf{I}, +}(x) \mathbf{c}_{\mathbf{n}}^{\mathbf{I}, +}$ where

$$\mathbf{S}_{\mathbf{n}}^{\mathbf{I}, +}(x) = \left(\tilde{T}_0(x) \mid S_{n_1}^{\circ, I_1, +}(x) \mid \cdots \mid S_{n_K}^{\circ, I_K, +}(x) \right), \tag{4.2}$$

$$S_{n_k}^{\circ, I_k, +}(x) = \left(v_0^{I_k}(x) \mid \tilde{u}_{-1}^{I_k}(x) \mid v_1^{I_k}(x) \mid \tilde{u}_0^{I_k}(x) \mid S_{n_k}^{\circ, I_k}(x) \right), \tag{4.3}$$

$$S_{n_k}^{\circ, I_k}(x) = \left(W_0^{I_k}(x) \mid \tilde{T}_1^{I_k}(x) \mid \cdots \mid W_{n_k}^{I_k}(x) \mid \tilde{T}_{n_k+1}^{I_k}(x) \right), \tag{4.4}$$

$$\mathbf{c}_{\mathbf{n}}^{\mathbf{I}, +} = \left(\tilde{c}_0 \mid (\mathbf{c}_{n_1}^{\circ, I_1})^\top \mid \cdots \mid (\mathbf{c}_{n_K}^{\circ, I_K})^\top \right)^\top, \tag{4.5}$$

$$\mathbf{c}_{n_k}^{\circ, I_k, +} = \left(c_{v_0^{I_k}} \mid c_{\tilde{u}_{-1}^{I_k}} \mid c_{v_1^{I_k}} \mid c_{\tilde{u}_0^{I_k}} \mid (\mathbf{c}_{n_k}^{\circ, I_k})^\top \right)^\top, \tag{4.6}$$

$$\mathbf{c}_{n_k}^{\circ, I_k} = \left(c_1^{I_k} \mid \tilde{c}_1^{I_k} \mid \cdots \mid c_{n_k+1}^{I_k} \mid \tilde{c}_{n_k+1}^{I_k} \right)^\top. \tag{4.7}$$

Unlike in $S_n^+(x)$, the sum spaces centred on each interval are ordered sequentially in $\mathbf{S}_n^{I,+}(x)$ rather than interleaving the Chebyshev polynomials/functions of the same degree across all the intervals. This is because each block in $\mathbf{S}_n^{I,+}(x)$ directly correlates to a block diagonal in the matrix after discretization, allowing for a clear decoupling of the problem. We denote the multiple-interval sum space by \mathbf{S}_n^I which is constructed as $\mathbf{S}_n^{I,+}$ but without the initial four terms $v_0^{I_k}(x), \tilde{u}_{-1}^{I_k}(x), v_1^{I_k}(x), \tilde{u}_0^{I_k}(x)$ at the start of each block in (4.3).

Similarly, we define the dual multiple-interval sum space $\mathbf{S}_n^{I,*}(x)$ as

$$\mathbf{S}_n^{I,*}(x) = \left(\tilde{U}_{-2}^{I_1}(x) \mid S_{n_1}^{\circ, I_1,*}(x) \mid \cdots \mid S_{n_K}^{\circ, I_K,*}(x) \right), \quad (4.8)$$

$$S_{n_k}^{\circ, I_k,*}(x) = \left(V_0^{I_k}(x) \mid \tilde{U}_{-1}^{I_k}(x) \mid \cdots \mid V_{n_k+2}^{I_k}(x) \mid \tilde{U}_{n_k+1}^{I_k}(x) \right). \quad (4.9)$$

In the next proposition we show that the multiple-interval sum space is also a frame. Let S^I denote the multiple-interval sum space

$$S^I := \text{span}(\{\tilde{T}_0^{I_1}, \tilde{T}_n^{I_k}, W_m^{I_k} : n \in \mathbb{N}, m \in \mathbb{N}_0, k = 1, \dots, K\}). \quad (4.10)$$

Proposition 4.1 (Multiple-interval frame). *Let $I = \cup_{k=1}^K I_k$ and suppose that the intervals only overlap on a set of measure zero. Denote the weight $\beta_k(x) = V_0^{I_k}(x)$ and $\beta = \sum_{k=1}^K \beta_k$. Then, the sum space S^I , for $x \in I$, is a frame on $L_\beta^2(I)$.*

The crux of the proof is to obtain the upper bound for the frame condition due to the global support of the functions $\tilde{T}_n^{I_k}(x)$ which overlap across all the user-chosen intervals. By utilizing the anti-self adjointness of the Hilbert transform and the fact that $\mathcal{H}[\tilde{T}_n](x) = -W_{n-1}(x)$, $n \geq 1$, we convert the boundedness of a function tested against $\tilde{T}_n^{I_k}(x)$ to the Hilbert transform of a related function tested against the compactly supported $W_{n-1}^{I_k}(x)$. Then, by utilizing classical boundedness results for the Hilbert transform on weighted Lebesgue spaces, we are able to obtain the desired result.

Proof. Consider any function $f \in L_\beta^2(I)$. We first obtain the lower bound as follows:

$$\begin{aligned} \|f\|_{L_\beta^2(I)}^2 &= \sum_{k=1}^K \|f\|_{L_\beta^2(I_k)}^2 = \sum_{k=1}^K \int_{I_k} (f\beta_k)^2 \beta_k^{-1} dx \\ &= \sum_{k=1}^K \sum_{n=0}^{\infty} |\langle f\beta_k, W_n^{I_k} \rangle_{L^2(I_k)}|^2 = \sum_{k=1}^K \sum_{n=0}^{\infty} |\langle f, W_n^{I_k} \rangle_{L_\beta^2(I_k)}|^2 \\ &\leq \sum_{n=0}^{\infty} \sum_{k=1}^K \left[|\langle f, \tilde{T}_n^{I_k} \rangle_{L^2(I)}|^2 + |\langle f, W_n^{I_k} \rangle_{L^2(I)}|^2 \right]. \end{aligned} \quad (4.11)$$

As the summands are non-negative, the swapping of the sums in the second inequality is justified by Fubini's theorem. We split the upper bound result into three steps. In the first step we note that, as shown in (4.11),

$$\sum_{n=0}^{\infty} \sum_{k=1}^K |\langle f, W_n^{I_k} \rangle_{L^2_{\beta}(I)}|^2 = \|f\|_{L^2_{\beta}(I)}^2. \quad (4.12)$$

For the second step, for $x \in I$, we denote $\gamma(x) := \sum_{k=1}^K W_0^{I_k}(x)$. Moreover, we denote the extension of γ to \mathbb{R} by $\tilde{\gamma}$ such that $\tilde{\gamma}$ is non-negative and satisfies the criterion for a Muckenhoupt A_2 weight, i.e. for any interval Y and a constant C independent of Y :

$$\sup_Y \frac{1}{|Y|^2} \left(\int_Y \tilde{\gamma} \, dx \right) \left(\int_Y \tilde{\gamma}^{-1} \, dx \right) \leq C < \infty. \quad (4.13)$$

Such a $\tilde{\gamma}$ exists, e.g. partition $\mathbb{R} \setminus I$ into a countable number of intervals $\{Y_j\}_{j=1}^{\infty}$:

$$\tilde{\gamma}(x) := \begin{cases} \gamma(x) & x \in I, \\ \sum_{j=1}^{\infty} W_0^{Y_j}(x) & x \notin I. \end{cases} \quad (4.14)$$

We note that β has compact support in I . Thus

$$\sum_{n=1}^{\infty} \sum_{k=1}^K |\langle f, \tilde{T}_n^{I_k} \rangle_{L^2_{\beta}(I)}|^2 = \sum_{n=1}^{\infty} \sum_{k=1}^K |\langle f, \tilde{T}_n^{I_k} \rangle_{L^2_{\beta}(\mathbb{R})}|^2 = \sum_{n=0}^{\infty} \sum_{k=1}^K |\langle \mathcal{H}[f\beta], W_n^{I_k} \rangle_{L^2(I)}|^2, \quad (4.15)$$

where the second equality follows from Proposition 3.2 and the fact that $W_n^{I_k}$ are supported on I_k . By applications of Fubini's theorem to swap the infinite and finite sums, as well as Parseval's identity, we note that

$$\sum_{n=0}^{\infty} \sum_{k=1}^K |\langle \mathcal{H}[f\beta], W_n^{I_k} \rangle_{L^2(I)}|^2 = \sum_{k=1}^K \int_{I_k} \mathcal{H}[f\beta]^2 W_0^{I_k} \, dx = \int_I \mathcal{H}[f\beta]^2 \gamma \, dx. \quad (4.16)$$

Since $\tilde{\gamma}$ is non-negative

$$\int_I \mathcal{H}[f\beta]^2 \gamma \, dx \leq \int_{\mathbb{R}} \mathcal{H}[f\beta]^2 \tilde{\gamma} \, dx \leq C \int_{\mathbb{R}} (f\beta)^2 \tilde{\gamma} \, dx, \quad (4.17)$$

for some constant $C > 0$ independent of f , where the second inequality follows from an application of the boundedness of the Hilbert transform on Lebesgue spaces with Muckenhoupt weights [25, Th. 9]. As β is supported on I

$$C \int_{\mathbb{R}} (f\beta)^2 \tilde{\gamma} \, dx = C \int_I (f\beta)^2 \gamma \, dx = C \sum_{k=1}^K \int_{I_k} f^2 \beta_k \, dx = C \|f\|_{L^2_{\beta}(I)}^2. \quad (4.18)$$

In the third step we deal with the term $\tilde{T}_0^{I_1}(x)$. We note that

$$\begin{aligned} |\langle f, \tilde{T}_0^{I_1} \rangle_{L_\beta^2(I)}|^2 &= \|f\beta\|_{L^1(I)}^2 \leq \|\beta^{1/2}\|_{L^2(I)}^2 \|f\beta^{1/2}\|_{L^2(I)}^2 \\ &= \left(\sum_{k=1}^K \int_{I_k} |\beta_k| dx \right) \|f\|_{L_\beta^2(I)}^2 = \left(\sum_{k=1}^K \frac{|I_k|\pi}{2} \right) \|f\|_{L_\beta^2(I)}^2 = \frac{|I|\pi}{2} \|f\|_{L_\beta^2(I)}^2, \end{aligned} \quad (4.19)$$

where the first inequality holds thanks to Hölder's inequality. Thus by (4.12) and (4.15)–(4.19), we note that the upper bound frame condition holds with the constant $(1 + C + |I|\pi/2)$. \square

From Proposition 3.7, we note that the operator $\mathcal{L}_{\mu,\lambda,\eta}$ maps a sum space centred on an interval I , to the dual sum space centred on the same interval. This observation leads to the following proposition.

Proposition 4.2 (Multiple-interval quasimatrix operators).

$$\begin{aligned} \mathbf{S}_n^I(x) &= \mathbf{S}_n^{I,*}(x)\mathbf{E}, \quad \mathcal{H}[\mathbf{S}_n^I](x) = \mathbf{S}_n^{I,*}(x)\mathbf{H}, \\ \frac{d}{dx}[\mathbf{S}_n^I](x) &= \mathbf{S}_n^{I,*}(x)\mathbf{D}^I, \quad \text{and } (-\Delta)^{1/2}[\mathbf{S}_n^I](x) = \mathbf{S}_n^{I,*}(x)\mathbf{A}^I, \end{aligned} \quad (4.20)$$

where $\mathbf{E}, \mathbf{H}, \mathbf{D}^I, \mathbf{A}^I \in \mathbb{R}^{(1+2N+6K) \times (1+2N+2K)}$ are the following block diagonal matrices:

$$\mathbf{E} = \begin{pmatrix} E & & & \\ & E^\dagger & & \\ & & \ddots & \\ & & & E^\dagger \end{pmatrix}, \quad \mathbf{H} = \begin{pmatrix} H & & & \\ & H^\dagger & & \\ & & \ddots & \\ & & & H^\dagger \end{pmatrix} \quad (4.21)$$

$$\mathbf{D}^I = \begin{pmatrix} D^{I_1} & & & \\ & D^{I_2,\dagger} & & \\ & & \ddots & \\ & & & D^{I_K,\dagger} \end{pmatrix}, \quad \mathbf{A}^I = \begin{pmatrix} A^{I_1} & & & \\ & A^{I_2,\dagger} & & \\ & & \ddots & \\ & & & A^{I_K,\dagger} \end{pmatrix}, \quad (4.22)$$

where the matrices $E^\dagger, H^\dagger, D^\dagger$, and A^\dagger are the matrices E, H, D , and A , respectively, as defined in Proposition 3.7, but with the first row and column removed.

Consider the truncated expansion of the right-hand side f in the dual multiple-interval sum space, $f(x) \approx \mathbf{S}_n^{I,*}\mathbf{f}$. As in the single interval case, the matrix $\mathbf{L} = \lambda\mathbf{E} + \mu\mathbf{H} + \eta\mathbf{D}^I + \mathbf{A}^I$ is rectangular and the linear system to find the coefficients, \mathbf{u} , of $u(x)$ in the multiple-interval sum space,

$$\mathbf{L}\mathbf{u} = \mathbf{f}, \quad \mathbf{L} \in \mathbb{R}^{(1+2N+6K) \times (1+2N+2K)} \quad (4.23)$$

is overdetermined. This issue is overcome by appending four extra columns to \mathbf{L} per interval. \mathbf{L} has the block diagonal structure:

$$\mathbf{L} = \begin{pmatrix} L^{I_1} & & & \\ & L^{I_2, \dagger} & & \\ & & \ddots & \\ & & & L^{I_K, \dagger} \end{pmatrix}, \quad (4.24)$$

where each block has four more rows than columns. Hence, we define the matrix \mathbf{L}^+ as

$$\mathbf{L}^+ = \begin{pmatrix} L^{I_1, +} & & & \\ & L^{I_2, \dagger, +} & & \\ & & \ddots & \\ & & & L^{I_K, \dagger, +} \end{pmatrix}, \quad (4.25)$$

where, for $k = 2, \dots, K$,

$$L^{I_1, +} = \left(\begin{array}{cccc|c} -\lambda & 0 & 0 & 0 & 0 \\ 0 & 1 & 0 & 0 & 0 \\ 0 & 0 & 1 & 0 & 0 \\ 0 & 0 & 0 & 1 & 0 \\ \lambda & 0 & 0 & 0 & 1 \\ 0 & 0 & 0 & 0 & 0 \\ \vdots & \vdots & \vdots & \vdots & \vdots \\ 0 & 0 & 0 & 0 & 0 \end{array} \right) L^{I_1, \circ}, \quad L^{I_k, \dagger, +} = \left(\begin{array}{cccc|c} 1 & 0 & 0 & 0 & \\ 0 & 1 & 0 & 0 & \\ 0 & 0 & 1 & 0 & \\ 0 & 0 & 0 & 1 & \\ 0 & 0 & 0 & 0 & \\ \vdots & \vdots & \vdots & \vdots & \\ 0 & 0 & 0 & 0 & \end{array} \right) L^{I_k, \dagger}, \quad (4.26)$$

where the nonzero entries are placed in the rows corresponding to $V_0^{I_k}$, $\tilde{U}_{-1}^{I_k}$, $V_1^{I_k}$, and $\tilde{U}_0^{I_k}$, respectively. We reiterate that symbol \circ denotes the matrix without its first column and \dagger denotes the matrix without its first column and row. The matrix $\mathbf{L}^+ \in \mathbb{R}^{(1+2N+6K) \times (1+2N+6K)}$ is square and we find the coefficients \mathbf{u}^+ , in the appended multiple-interval sum space, of the solution $u(x)$ to (\star) by solving the following system:

$$\mathbf{L}^+ \mathbf{u}^+ = \mathbf{f}. \quad (4.27)$$

Since \mathbf{L}^+ is block diagonal, the solve can be reduced to solving K linear systems for each (much smaller) block, $k = 2, \dots, K$,

$$L^{I_1, +} \mathbf{u}^{I_1, +} = \mathbf{f}^{I_1}, \quad L^{I_k, \dagger, +} \mathbf{u}^{I_k, +} = \mathbf{f}^{I_k}. \quad (4.28)$$

Moreover, the linear systems are independent and can be solved in parallel.

5 Implementation notes

5.1 Expansion

As the family of approximating functions is not orthogonal, the expansion of a known function, $f(x)$, in the sum space or its dual is nontrivial. In particular, the expansion of a general function need not be unique. For our purposes, we desire an expansion that approximates our known function to the required tolerance and the coefficients of the expansion are (relatively) small in magnitude.

Aside from the known function f being an obvious composition of the functions in $\mathbf{S}_n^I(x)$, there are two cases to consider:

1. f is compactly supported on the real line and the intervals $I_k = [a_k, b_k]$, $k = 1, \dots, K$, are chosen such that either $f(x) \rightarrow 0$ or $|f(x)| \rightarrow \infty$ as $x \rightarrow a_k$ and $x \rightarrow b_k$;
2. Any function that does not fit under the first case.

In the first case, if $f(x) \rightarrow 0$ at the endpoints of the interval I_k for some $k \in \{1, \dots, K\}$, then it might be well approximated in that interval by an expansion in $W_n^{I_k}(x)$. Similarly, if f blows up at the interval endpoints it might be well represented by an expansion in $V_n^{I_k}(x)$. The advantage of only expanding $f(x)$ in $W_n^{I_k}(x)$ and $V_n^{I_k}(x)$ is that the coefficients of the expansion can be quickly computed to any given tolerance with an adaptive algorithm based on the discrete cosine transform that takes $\mathcal{O}(Kn \log n)$ for n coefficients and K intervals [5, 21]. If we partially expand $f(x)$ in $V_n^{I_k}(x)$ for some k , but we require the expansion in the dual sum space, we utilize the identity mappings as defined in Propositions 3.7 and 4.2.

For functions that are not contained in the first case, we turn to the techniques used in *frame* theory [2]. Essentially, we find the coefficients of the expansion that optimally interpolate the values of $f(x)$ (or a linear operator applied to f) at a set of collocation points in a least squares sense. Consider the collocation points $\mathbf{x} = (x_1, \dots, x_M)$. We note that the set of collocation points should include points outside the intervals in order to ensure the tails also match. The least-squares matrix for the dual sum space is given by:

$$\mathbf{G}_{ij} = [l_i[\mathbf{S}_n^{I,*}]]_j, \quad i = 1 \dots, M, \quad j = 1, \dots, 1 + 2N + 6K, \quad (5.1)$$

where $\{l_i\}$ are a set of linear operators. Common choices include the identity, e.g. $l_i[\mathbf{S}_n^{I,*}] = \mathbf{S}_n^{I,*}(x_i)$ or linear operators designed to emulate Riemann sums $l_i[\mathbf{S}_n^{I,*}] = (x_{i+1} - x_{i-1})\mathbf{S}_n^{I,*}(x_i)$. Similarly we compute $\mathbf{b}_i = l_i[f]$ and we solve the following least-squares problem for the

expansion coefficients \mathbf{f} :

$$\min_{\mathbf{f}} \|\mathbf{G}\mathbf{f} - \mathbf{b}\|_2, \quad (5.2)$$

so that $f(x) \approx \mathbf{S}_n^{I,*}(x)\mathbf{f}$. The same technique can be used to find expansions in $\mathbf{S}_n^I(x)$. It is well known that the least-squares matrix is ill-conditioned for increasing M , K and n . However, we still recover suitable least squares solutions if we sufficiently oversample the collocation points and an adequate SVD solver is used. We refer to the work of Adcock and Huybrechs for further details [2, 3].

5.2 Approximate identity map from $S_n^+(x)$ to $S_n^*(x)$

In our method, we find the approximate solution expanded in the appended sum space. A requirement in some problems is to reuse the computed solution as part of the right-hand side of the next solve. Hence, after each solve, we must map the appended sum space expansion of our current iterate to the expansion in the dual sum space. Propositions 3.7 and 4.2 provide identity mappings for the sum space. Hence, it remains to map the coefficients of the functions found in the appended sum space that are not in the sum space.

We outline the approach when utilizing a single interval at $[-1, 1]$ in the solver and briefly mention the extension to multiple intervals. Given \mathbf{u}^+ , the goal is to find the coefficient vector, \mathbf{u}^* , such that

$$u(x) \approx S_n^+(x)\mathbf{u}^+ = S_n^*(x)\mathbf{u}^*. \quad (5.3)$$

The first step is to expand the four functions $v_0(x)$, $\tilde{u}_{-1}(x)$, $v_1(x)$ and $\tilde{u}_0(x)$ in the sum space and collect the coefficients in the vectors \mathbf{v}_0 , $\tilde{\mathbf{u}}_{-1}$, \mathbf{v}_1 , and $\tilde{\mathbf{u}}_0$, respectively. Next we form the identity mapping from $S_n^+(x)$ to $S_n(x)$, denoted $R \in \mathbb{R}^{(2n+3) \times (2n+7)}$, as follows:

$$R := \begin{pmatrix} 1 & | & | & | & | & 0 & \dots \\ 0 & \mathbf{v}_0 & \tilde{\mathbf{u}}_{-1} & \mathbf{v}_1 & \tilde{\mathbf{u}}_0 & \vdots & I_{2n+2} \\ \vdots & | & | & | & | & & \end{pmatrix}. \quad (5.4)$$

Essentially R is constructed by assembling the $(2n+3) \times (2n+3)$ identity matrix and adding the four coefficient vectors, of the additional functions, in R between the first and second columns. The approximate identity operator B such that $S_n^+(x) \approx S_n^*(x)B$ is defined as

$$B := ER, \quad (5.5)$$

where E is the identity operator from $S_n(x)$ to $S_n^*(x)$ as defined in Proposition 3.7.

For multiple intervals, we denote the identity mapping as $\mathbf{R} \in \mathbb{R}^{(1+2N+2K) \times (1+2N+6K)}$, $\mathbf{R} : \mathbf{S}_n^{I,+}(x) \rightarrow \mathbf{S}_n^I(x)$, where K is the number of intervals and consists of the identity matrix with an additional $4K$ dense columns in the positions of the additional functions in the appended sum space. As before, we define $\mathbf{B} := \mathbf{ER}$ so that $\mathbf{S}_n^{I,+}(x) \approx \mathbf{S}_n^{I,*}(x)\mathbf{B}$.

6 Numerical examples

In this section we provide several numerical examples. During numerical experiments, we found that approximating with a sum space centred at a single interval was normally insufficient for satisfying the condition $u(x) \rightarrow \infty$ as $|x| \rightarrow \infty$. However, this was resolved when utilizing a combination of sum spaces centred at multiple intervals. In particular, we found that five intervals worked well in all examples. Unless the initial condition or right-hand side are represented exactly by the (dual) sum space, we find the coefficient vectors via the truncated least-squares matrix as explained in Section 5.1.

Code availability: For reproducibility, an implementation of the spectral method as well as scripts to generate the plots and solutions can be found at <https://github.com/ioannisPpapadopoulos/SumSpaces.jl>. The version of the software used in this paper is archived on Zenodo [34, 35].

6.1 Manufactured solutions

In order to test the spectral convergence of our method, our first example is constructed via the method of manufactured solutions. We fix the exact solution $u(x) = e^{-x^2}$. Note that $\frac{d}{dx}e^{-x^2} = -2xe^{-x^2}$. Moreover [39, Prop. 4.2],

$$(-\Delta)^{1/2}u(x) = \frac{2}{\sqrt{\pi}} {}_1F_1(1; 1/2; -x^2), \quad (6.1)$$

where ${}_1F_1$ denotes the Kummer confluent hypergeometric function [36, Sec. 16.2]. An integration of (6.1) reveals that

$$\mathcal{H}[u](x) = -\frac{i}{x} \left(e^{-x^2} |x| \operatorname{erf}(i|x|) \right), \quad \operatorname{erf}(z) := \frac{2}{\sqrt{\pi}} \int_0^z e^{-t^2} dt. \quad (6.2)$$

In the first case we set $\lambda = 1$, $\mu = \eta = 0$:

$$(\mathcal{I} + (-\Delta)^{1/2})u(x) = e^{-x^2} + \frac{2}{\sqrt{\pi}} {}_1F_1(1; 1/2; -x^2). \quad (6.3)$$

In the second case we have $\lambda = \mu = \eta = 1$:

$$\begin{aligned} & (\mathcal{I} + \frac{d}{dx} + \mathcal{H} + (-\Delta)^{1/2})u(x) \\ &= (1 - 2x)e^{-x^2} - \frac{i}{x} \left(e^{-x^2} |x| \operatorname{erf}(i|x|) \right) + \frac{2}{\sqrt{\pi}} {}_1F_1(1; 1/2; -x^2). \end{aligned} \quad (6.4)$$

For this example we fix five intervals at $[-5, -3]$, $[-3, -1]$, $[-1, 1]$, $[1, 3]$, and $[3, 5]$. In the least-squares expansion we choose 6001 equally spaced points on each interval as well as 6001 equally spaced points between $[-25, -5]$ and $[5, 25]$. This results in 42,001 unique collocation points. We choose the appended sum space functions $v_0(x)$, $\tilde{u}_{-1}(x)$, $v_{n+2}(x)$, $\tilde{u}_{n+1}(x)$ centred on each interval. As discussed in Remark 3.6, this improves the conditioning of the induced linear systems and helps to ensure that the convergence rate is not polluted by numerical instabilities due to ill-conditioning. An FFT proved too inaccurate for spectral convergence. Hence, the additional functions are approximated by approximating the necessary inverse Fourier transforms via Mathematica's `NIntegrate` routine [27].

In Fig. 3, we provide spy plots of the induced subblocks of \mathbf{L}^+ . We see that the matrices are sparse and almost banded. A semi-log plot of the convergence for both cases is depicted in Fig. 4. The error is measured in the l^∞ -norm as measured on a 1001-point equally spaced grid at $[-5, 5]$, i.e.

$$\max_{x \in \{-5, -4.99, \dots, 4.99, 5\}} |u(x) - \mathbf{S}_n^I(x)\mathbf{u}|. \quad (6.5)$$

The convergence is spectral. We note that the error stagnates around 10^{-14} in Fig. 4a and 10^{-13} in Fig. 4b as the error of the approximation of the right-hand side stagnates at the same magnitude.

Since we are not guaranteed that the sum space is a frame on all \mathbb{R} (Proposition 4.1 only guarantees it is a frame on the user-chosen intervals), in Fig. 5 we investigate the behaviour of the expansion coefficients of the right-hand side. In particular we plot the l^∞ -norm of the coefficient vector \mathbf{f} of the right-hand sides (6.3) and (6.4) for increasing truncation degree n . Despite the lack of a strict frame condition, we achieve bounded coefficients of magnitude $\mathcal{O}(1)$ for all values of n .

6.2 Discontinuous right-hand side

This example examines the behaviour of the (dual) sum space approximation of a problem with discontinuous data. We seek $u \in H^{1/2}(\mathbb{R})$ that satisfies

$$(\mathcal{I} + (-\Delta)^{1/2})u(x) = f(x), \quad \text{where } f(x) := \begin{cases} 1 & |x| < 1, \\ 0 & |x| \geq 1. \end{cases} \quad (6.6)$$

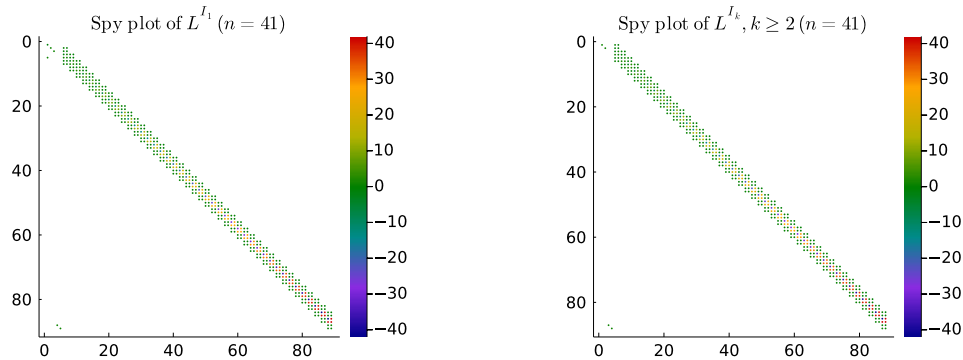


Figure 3: Spy plots of the matrices in the linear systems after discretizing and decoupling (6.4) interval-wise. Here $\lambda = \eta = \mu = 1$ and we use the additional functions $v_0, \tilde{u}_{-1}, v_{n+1}, \tilde{u}_{n+1}$. The matrices are sparse and almost banded.

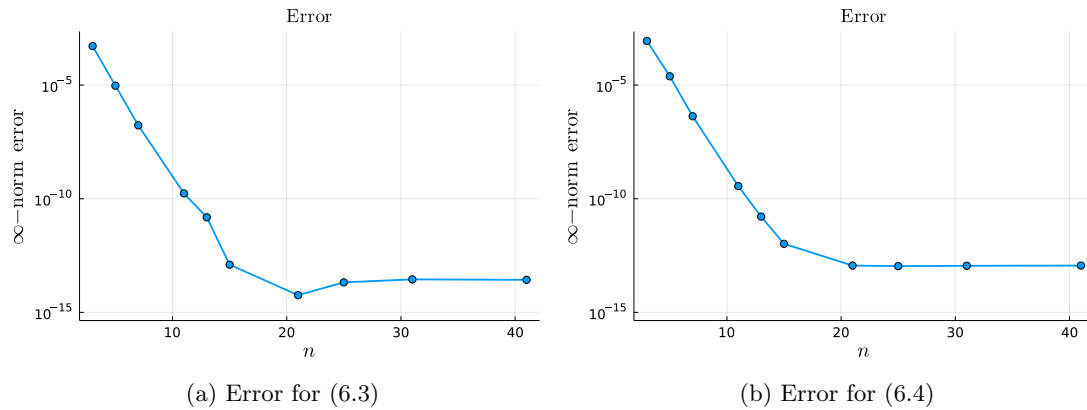


Figure 4: Error in the numerical solution $u(x)$ as measured by (6.5) with the right-hand sides (6.3) and (6.4) for increasing truncation degree n . The convergence is spectral.

We use a multiple-interval (dual) sum space centred at the intervals $[-5, -3]$, $[-3, -1]$, $[-1, 1]$, $[1, 3]$, and $[3, 5]$. In the sum space expansion we choose 6001 equally spaced points on each interval as well as 6001 equally spaced points between $[-10, -5]$ and $[5, 10]$. This results in 42,001 unique collocation points. As the multiple-interval dual sum space contains functions that are undefined at $x = -5, -3, -1, 1, 3$ and 5 , we instead choose 6001 equally spaced points in $[a + \epsilon, b - \epsilon]$, $\epsilon = 10^{-2}$, where a, b represent the endpoints of each interval as well as 6001 equally spaced points in $[-10 + \epsilon, -5 - \epsilon]$ and $[5 + \epsilon, 10 - \epsilon]$. This results in 42,007 collocation points.

We first check the convergence of the approximation of the discontinuous right-hand side f . We measure the error in the sum space approximation via (6.5). We exclude

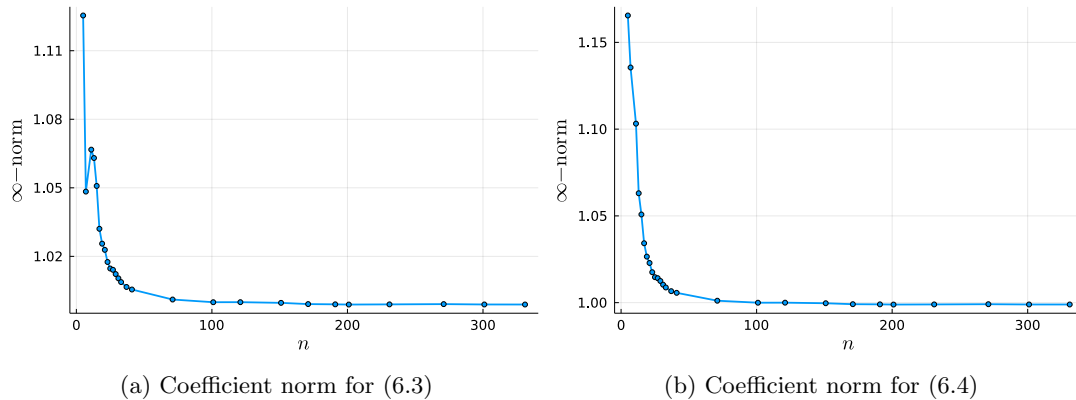


Figure 5: The l^∞ -norm of the coefficient vector of the sum space expansion of the right-hand side for increasing truncation degree n .

the points $x = -5, -3, -1, 1, 3$ and 5 , when measuring the error in the dual sum space expansion, i.e. we compute:

$$\max_{x \in \{-5, -4.99, \dots, 4.99, 5\} \setminus \{-5, -3, -1, 1, 3, 5\}} |u(x) - \mathbf{S}_n^{\mathbf{I},*}(x)\mathbf{u}|. \quad (6.7)$$

In Fig. 6, we plot the sum space approximated right-hand side as well as the error plot with increasing truncation degree of both the sum space and dual sum space approximations. At truncation degree $n = 101$, the sum space error is of the order $\mathcal{O}(10^{-6})$. Whereas the dual sum space approximation reaches an error of $\mathcal{O}(10^{-13})$. Hence, the best approximation of this particular discontinuous right-hand side is achieved via a direct dual sum space expansion rather than a sum space expansion coupled with the identity conversion operator \mathbf{E} (as defined in (4.21)) to re-expand in the dual sum space.

The numerical solution is plotted in Fig. 7 as well as an approximation of the convergence. The appended sum space functions are $v_0(x)$, $\tilde{u}_{-1}(x)$, $v_{n+2}(x)$, and $\tilde{u}_{n+1}(x)$. Mathematica's `NIntegrate` routine is used to compute the necessary inverse Fourier transforms. As we do not have an explicit solution, we cannot measure the error directly. Instead, we truncate the right-hand side expansion at degrees $n_f = 11, 15, 21$, and 27 . We then measure the 2-norm difference in the sum space coefficient vectors at truncation degree n and $n - 2$ of the solution for $n = n_f + 2, n_f + 4, \dots, n_f + 16$. We observe spectral convergence in the coefficient vectors.

As in the previous example, we investigate the behaviour of the expansion coefficients in both the sum space and dual sum space for increasing degree n in Fig. 8. The result is interesting; the norm begins large and appears to blow-up, reaching a magnitude of $\mathcal{O}(10^{10})$ at $n = 17$ for the sum space expansion and $\mathcal{O}(10^6)$ at $n = 13$ for the dual

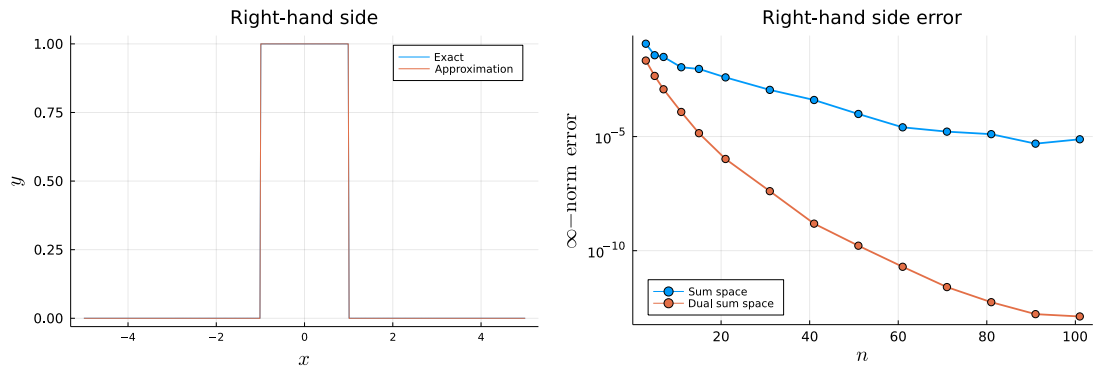


Figure 6: The exact and sum space approximated $f(x)$ as defined in (6.6) ($n = 41$) (left) and the l^∞ -norm error semi-log plot for the approximation of $f(x)$ for increasing truncation degree n (right). We use the error measure (6.5) for the sum space approximation and (6.7) for the dual sum space approximation.

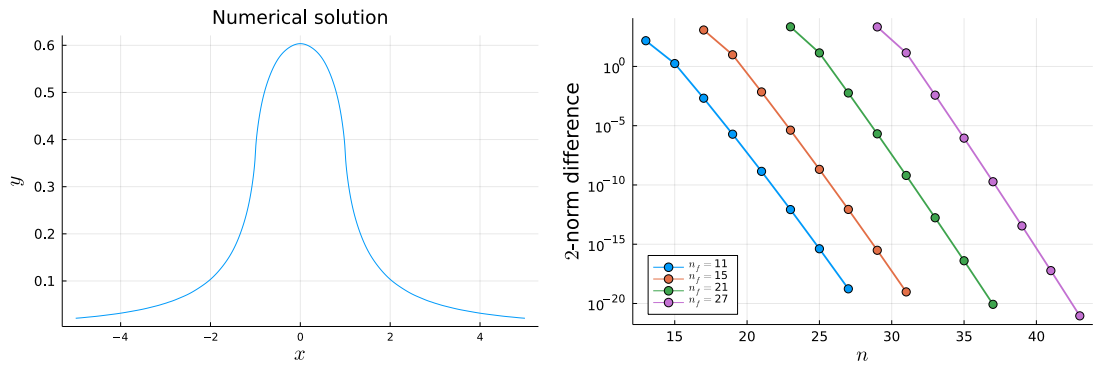


Figure 7: Numerical approximation of the solution to (6.6), $n = 41$ (left). l^2 -norm difference of the coefficients of the expansion of the solution, where we fix the right-hand side expansion at degree $n_f = 11, 15, 21$, and 27 (right).

sum space expansion. Thereafter, the norm oscillates in the sum space expansion until $n = 41$ where afterwards the norm drops at an exponential rate. For $n > 300$ the norm has magnitude $\mathcal{O}(1)$. In the dual sum space expansion, the norm quickly decreases for $n > 13$ and plateaus for $n \geq 71$ at a value of magnitude of $\mathcal{O}(10^{-1})$.

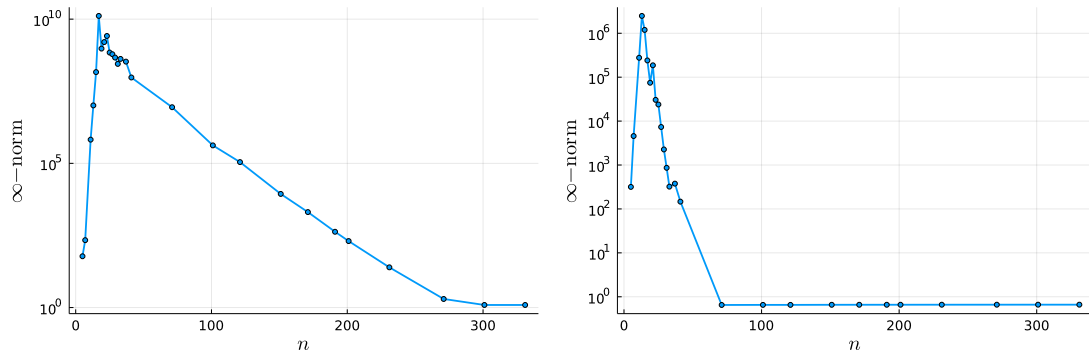


Figure 8: The l^∞ -norm of the coefficient vectors of the sum space expansion (left) and the dual sum space expansion (right) of (6.6) for increasing truncation degree n .

6.3 Nonsmooth right-hand side

Here we conduct the same investigation as in the previous example except now we choose the right-hand side

$$f(x) = \begin{cases} \arcsin(x) & \text{if } |x| \leq 1, \\ \arcsin(1)\operatorname{sgn}(x)e^{1-|x|} & \text{otherwise.} \end{cases} \quad (6.8)$$

We use the same multiple-interval sum space as in the previous example as well as the same collocation points for the (dual) sum space expansion.

In Fig. 9 we plot the approximation of $f(x)$ expanded in the sum space at truncation degree $n = 41$ together with a plot of the exact right-hand side. Moreover, we plot the convergence of the expansions of $f(x)$. The error norms are measured with the same metrics as in the previous example. Both expansions appear to stagnate at an error of $\mathcal{O}(10^{-8})$. For smaller truncation degree values of n the error in the dual sum space expansions is smaller, however, at $n = 101$, the sum space expansion has the smallest error.

The appended sum space functions are $v_0(x)$, $\tilde{u}_{-1}(x)$, $v_{n+2}(x)$, and $\tilde{u}_{n+1}(x)$. Mathematica's `NIntegrate` routine is used to compute the necessary inverse Fourier transforms. In Fig. 10 we plot the numerical solution $u(x)$ of (\star) (where $\lambda = 1$, $\mu = \eta = 0$). Again as we do not have an explicit solution, we truncate the right-hand side expansion at degree $n_f = 11, 15, 21$, and 27 . We then measure the 2-norm difference in the sum space coefficient vectors at truncation degree n and $n - 2$ of the solution for $n = n_f + 2, n_f + 4, \dots, n_f + 16$. We observe spectral convergence in the coefficient vectors.

As in the previous two examples, we investigate the behaviour of the expansion coefficients in both the sum space and dual sum space for increasing degree n in Fig. 11.

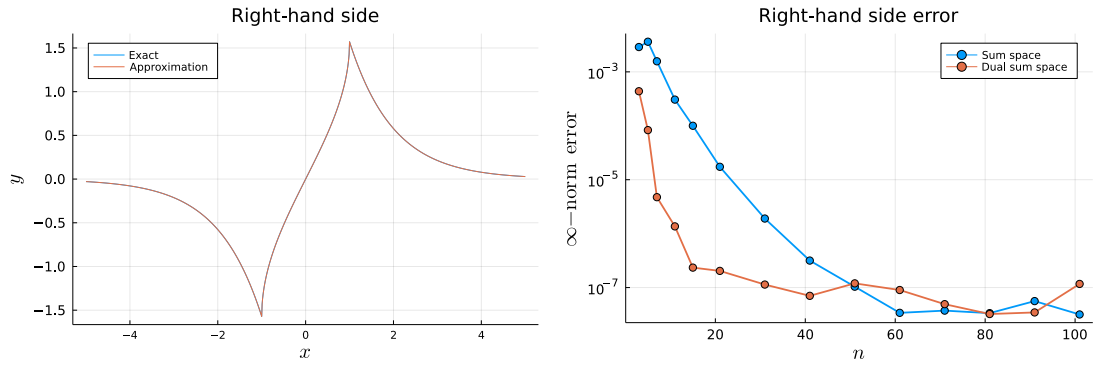


Figure 9: The exact and sum space approximated $f(x)$ as defined in (6.8) ($n = 41$) (left) and the l^∞ -norm error semi-log plot for the approximation of $f(x)$ for increasing truncation degree n (right). We use the measure (6.5) for the sum space approximation and (6.7) for the dual sum space approximation.

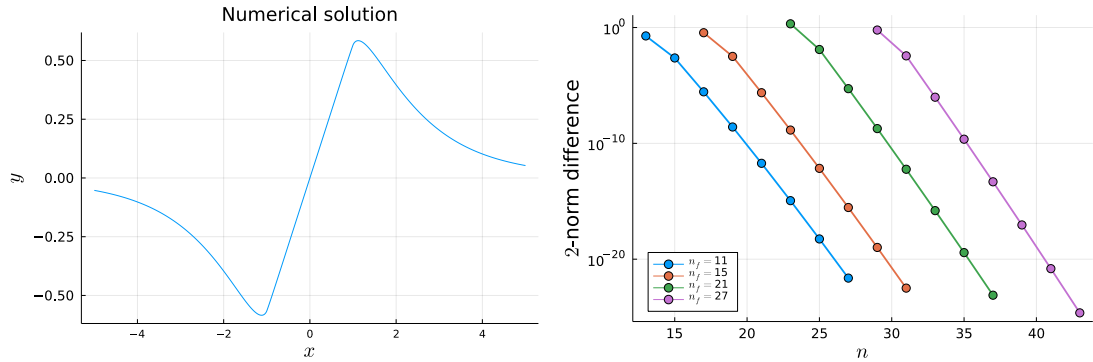


Figure 10: Numerical approximation of the solution to the nonsmooth right-hand side problem, $n = 41$ (left). l^2 -norm difference of the coefficients of the expansion of the solution, where we fix the right-hand side expansion at degree $n_f = 11, 15, 21$ and 27 (right).

As in the discontinuous right-hand side example, the l^∞ -norm of the coefficient vector begins large and appears to blow-up, reaching a magnitude of approximately $\mathcal{O}(10^6)$ at $n = 17$ for the sum space expansion and $\mathcal{O}(10^5)$ at $n = 13$ for the dual sum space expansion. Thereafter, the norm decreases and for $n \geq 71$ plateaus around $\mathcal{O}(10^4)$ in both expansions.

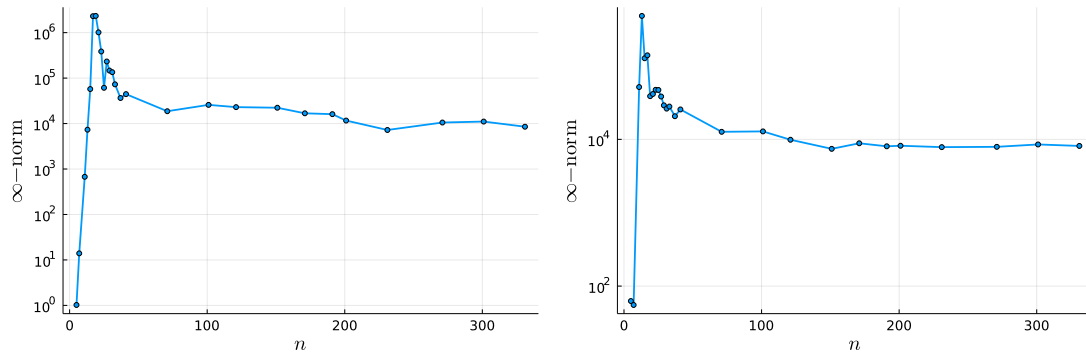


Figure 11: The l^∞ -norm of the coefficient vector of the sum space (left) and the dual sum space (right) expansions of (6.8) for increasing truncation degree n .

6.4 Fractional heat equation

Consider the fractional heat equation, i.e. the following time-dependent fractional PDE:

$$\partial_t u(x, t) + (-\Delta)^{1/2} u(x, t) = 0, \quad u(x, t) \rightarrow 0 \text{ as } |x| \rightarrow \infty. \quad (6.9)$$

We pick the following two choices for the initial condition:

$$u(x, 0) = (x^2 + 1)^{-1}, \quad (6.10)$$

$$u(x, 0) = W_0(x). \quad (6.11)$$

The initial condition (6.10) coincides with a constant scaling of the fundamental solution, $t(2\pi(x^2 + t^2))^{-1}$, to the fractional heat equation at $t = 1$ [46, Sec. 2]. Hence, (6.9) with the initial condition (6.10) has the exact solution:

$$u(x, t) = \frac{1 + t}{x^2 + (1 + t)^2}. \quad (6.12)$$

We discretize (6.9) in time with a backward Euler discretization to yield, for $k \geq 0$,

$$\begin{aligned} \lambda u_{k+1}(x) + (-\Delta)^{1/2} u_{k+1}(x) &= \lambda u_k(x), \\ u_{k+1}(x) &\rightarrow 0 \text{ as } |x| \rightarrow \infty, \end{aligned} \quad (6.13)$$

where $u_0(x) = (x^2 + 1)^{-1}$ or $W_0(x)$ and $\lambda = (\Delta t)^{-1}$ where Δt is the time step. By choosing $\mu = \eta = 0$, we recover the equation (\star) which is discretized in space using our spectral method. We choose the appended sum space functions $v_0(x)$, $\tilde{u}_{-1}(x)$, $v_1(x)$, and $\tilde{u}_0(x)$. We use an FFT (as outlined in Appendix A) to approximate the necessary inverse Fourier transforms.

Given the tuple of intervals \mathbf{I} and the coefficient vector solution \mathbf{u}_k at time step iterate k , we solve the following for the coefficient vector solution \mathbf{u}_{k+1} :

$$(\lambda \mathbf{E} + \mathbf{A}^{\mathbf{I}})\mathbf{u}_{k+1} = \lambda(\mathbf{E}\mathbf{R})\mathbf{u}_k. \quad (6.14)$$

\mathbf{E} and $\mathbf{A}^{\mathbf{I}}$ are defined in Proposition 4.2 and \mathbf{R} is defined in Section 5.2. We reiterate that $(\lambda \mathbf{E} + \mathbf{A}^{\mathbf{I}})$ is block diagonal. Hence, after the right-hand side $\lambda(\mathbf{E}\mathbf{R})\mathbf{u}_k$ is computed, we decompose the solve into K smaller linear solves, where K is the number of intervals, as in (4.28). Our approximate solution is given by

$$u(x, k\Delta t) \approx \mathbf{S}_n^{\mathbf{I},+}(x)\mathbf{u}_k. \quad (6.15)$$

We pick the multiple-interval sum space centred at the intervals $[-5, -3]$, $[-3, -1]$, $[-1, 1]$, $[1, 3]$, and $[3, 5]$. We fix the truncation degree $n = 5$. The initial condition (6.10) is expanded in the sum space via the least-squares matrix as discussed in Section 5.1. We use 5001 equally spaced points in the interval $[-5, 5]$ and 501 equally spaced points in $[-20, -5]$ and $[5, 20]$ each. This results in 26,001 collocation points. The initial condition (6.11) is represented exactly as one of the intervals is $[-1, 1]$, resulting in zero initial error. We choose a time step of $\Delta t = 10^{-2}$. Snapshots of the solution at $t = 0, 1/2$ and 1 are found in Fig. 13b and contour plots of t against x are given in Fig. 14.

In Fig. 15 we estimate the errors of our numerical solutions. In Fig. 15a we compare our numerical solution with the exact solution (6.12). An exact solution for the initial condition (6.11) is not available. Hence, in Fig. 15b, we compare our approximate solution with one computed via an approximate inverse Fourier transform at each time step. By using that $\mathcal{F}[W_0] = \pi J_1(|\omega|)/|\omega|$ and an induction argument, one can show that (6.13) has the solution

$$u_{k+1}(x) = \mathcal{F}^{-1} \left[\frac{\pi J_1(|\omega|)}{|\omega|(1 + \lambda^{-1}|\omega|)^{k+1}} \right]. \quad (6.16)$$

For each iteration k , we approximate the solution $u_k(x)$ with an FFT as outlined in Appendix A. For 100 iterations, this took 92.2 seconds. By contrast, 100 solves of (6.14) took 0.0162 seconds. The setup took 6.95 seconds to compute the four FFTs to approximate the solutions required to construct the appended sum space $\mathbf{S}_n^{\mathbf{I},+}(x)$ (as all the intervals have the same width) and another 1.06 seconds to compute their expansions in the sum space $\mathbf{S}_n^{\mathbf{I}}(x)$. This totals to 8.01 seconds, approximately an 11 times speedup. We note that the setup is not tied to the initial condition or knowledge of its Fourier transform. Hence, after one initial setup, the time evolution of any initial condition can be computed in fractions of a second via the repeated solve of (6.14). The l^∞ -norm error is measured on a 1001-point equally spaced grid at $[-20, 20]$, i.e.

$$\max_{x \in \{-20, -19.99, \dots, 19.99, 20\}} |u(x) - \mathbf{S}_n^{\mathbf{I}}(x)\mathbf{u}|. \quad (6.17)$$

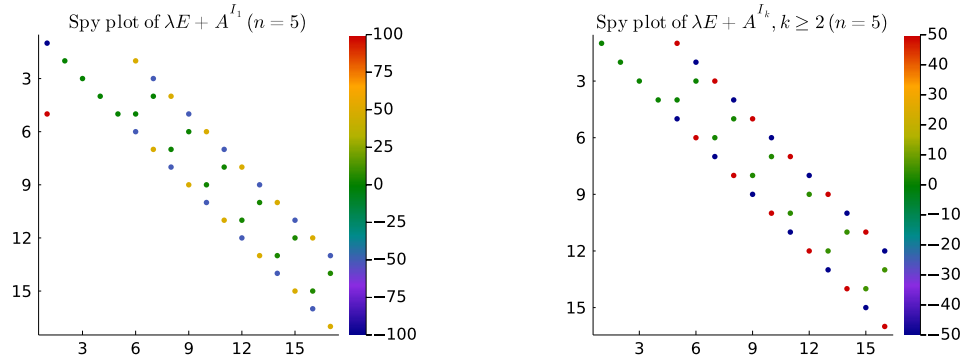


Figure 12: Spy plots of the matrices in the linear systems after decomposing (6.14) block-wise with $\lambda = 100$ and using the additional functions $v_0, \tilde{u}_{-1}, v_1, \tilde{u}_0$. The matrices are banded and sparse.

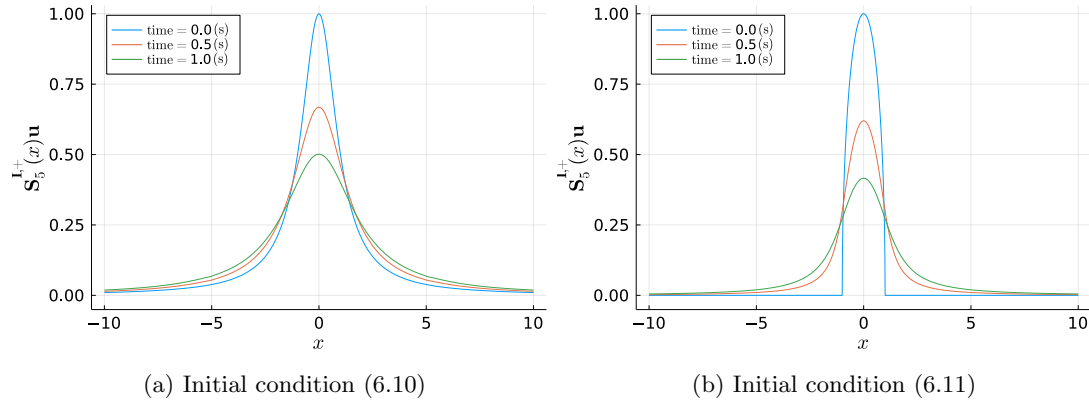


Figure 13: Snapshots of the numerical solutions of the fractional heat equation at $t = 0, 0.5$, and 1 using the truncated space $\mathbf{S}_5^{I,+}(x)$, $\Delta t = 10^{-2}$.

6.5 Wave propagation

Consider the fractional Hilbert wave equation:

$$[(-\Delta)^{1/2} + \mathcal{H} + \frac{\partial^2}{\partial t^2}]u(x, t) = f(x, t). \quad (6.18)$$

After a Fourier transform with respect to t , we recover the equation

$$[(-\Delta)^{1/2} + \mathcal{H} - \omega^2]\hat{u}(x, \omega) = \hat{f}(x, \omega). \quad (6.19)$$

Equation (6.19) is of the form (\star) with $\lambda = -\omega^2$, $\mu = 1$, and $\eta = 0$. Thus the idea is to solve (6.19) to find $\hat{u}(x, \omega)$, for a range of values of ω , and then take the inverse Fourier

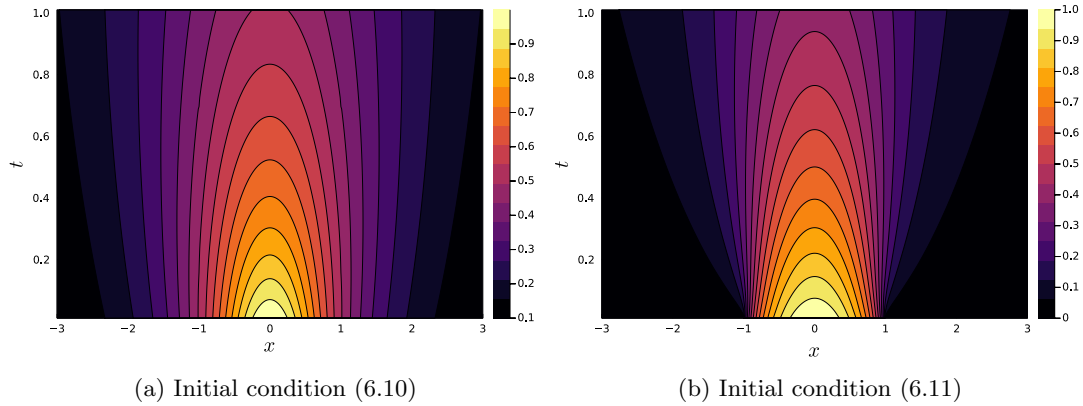
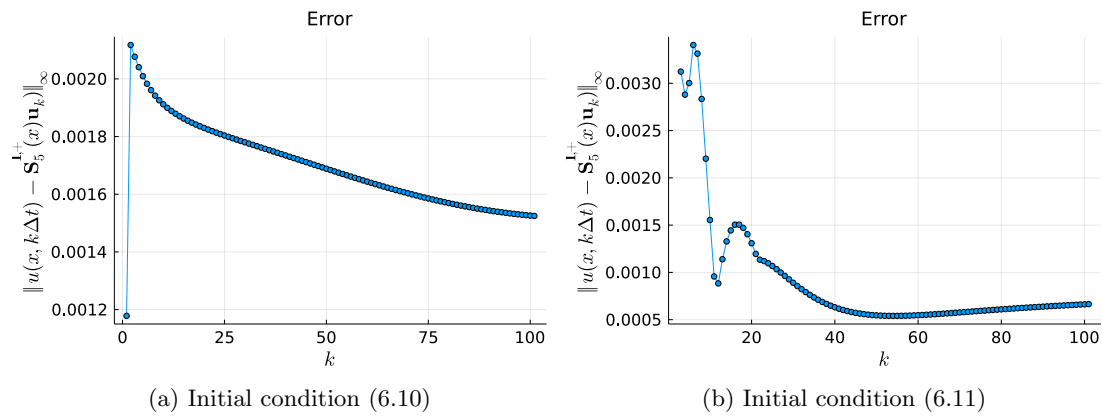


Figure 14: Contour plots of the numerical solutions to the fractional heat equation.

Figure 15: Error as measured by (6.17) of the numerical solutions to the fractional heat equation for iterate k as measured against (a) the exact solution and (b) the approximate FFT solution.

transform to recover the approximation of the physical solution $u(x, t)$. We choose the datum

$$f(x, t) = W_4(x)e^{-t^2} \implies \hat{f}(x, \omega) = \sqrt{\pi}W_4(x)e^{-\omega^2/4}. \quad (6.20)$$

This corresponds to a forcing term supported on $x \in [-1, 1]$ that exponentially decays in time.

To fix a unique solution, we enforce that $\lim_{|x| \rightarrow \infty} \hat{u}(x, \omega) \rightarrow 0$. For this example, we approximate the additional functions $\tilde{u}_{-1}(x)$, $\tilde{u}_{n+1}(x)$, $v_0(x)$ and $v_{n+2}(x)$ via an FFT (as described in Appendix A). We pick $n = 7$ and a uniform distribution of ω in the range $[0, 20]$ in increments of $1/10$. The inverse Fourier transform from $\hat{u}(x, \omega)$ to $u(x, t)$

is approximated via an FFT. We provide the contour plots of the approximate solutions of $\hat{u}(x, \omega)$ and $u(x, t)$ in Fig. 16. Even though the right-hand side is even, there is a drift in the solution $u(x, t)$ caused by the Hilbert transform operator. Note that the Hilbert transform maps even functions to odd functions and vice versa.

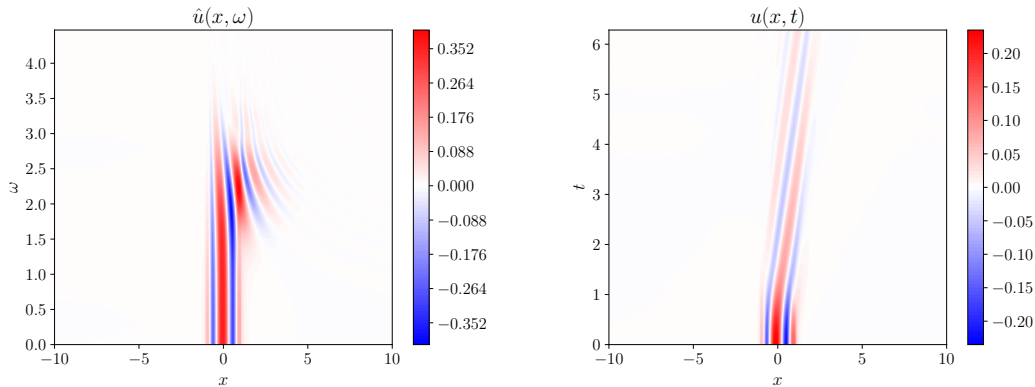


Figure 16: Contour plot of the approximation of $\hat{u}(x, \omega)$ (left) and $u(x, t)$ (right) with $f(x, t) = W_4(x)e^{-t^2}$ to the fractional Hilbert wave equation.

7 Conclusions

In this work we introduced a sparse spectral method for a one-dimensional fractional PDE posed on an unbounded domain that may contain the identity, Hilbert, derivative, and sqrt-Laplacian operators. The method is constructed by forming a sum space of weighted Chebyshev polynomials of the second kind extended to the whole of \mathbb{R} by zero and their Hilbert transforms. We derive explicit identities for the actions of the identity, Hilbert, derivative, and sqrt-Laplacian operators which allows us to build our method. The operator applied to different affine transformations of the sum spaces decouples during the solve. Hence, the solve can be performed in parallel over each interval separately. Moreover, the induced matrices are sparse leading to fast sparse solves. Numerically, we observe spectral convergence when the data is smooth. We emphasize that the coupling of the different interval sum spaces occurs during the expansion of the right-hand side.

In future work we plan to orthogonalize the basis as well as extend the method to general fractional Laplacians, $(-\Delta)^s$, $s \in (0, 1)$ by considering weighted Jacobi polynomials and their fractional Laplacian analogues. Moreover, by considering Zernike polynomials, the spectral method will be extended to two-dimensional problems posed on a disc.

Appendices

A Approximate inverse Fourier transform via the FFT

The setup of the spectral method requires four inverse Fourier transforms per interval. Although this can be reduced if the intervals are translations on \mathbb{R} and are of the same size as resulting solutions are simply the equivalent translations. In this section we describe how to use the FFT to approximate the inverse Fourier transform. The FFT implements the discrete Fourier transform (DFT) or its inverse (IDFT) with $\mathcal{O}(N \log N)$ complexity where N is the size of the input vector. Consider a vector $\mathbf{u} \in \mathbb{R}^N$. We denote the IDFT as \mathcal{F}_D^{-1} and define it as (as implemented in `ifft` of `FFTW.jl`):

$$\mathcal{F}_D^{-1}[\mathbf{u}]_j := \frac{1}{N} \sum_{n=1}^N \exp\left(i \frac{2\pi(j-1)(n-1)}{N}\right) \mathbf{u}_n, \quad j = 1, \dots, N. \quad (\text{A.1})$$

Suppose that N is even. Then, we also define the shifted IDFT, $\hat{\mathcal{F}}_D^{-1}$ such that the components of $\mathcal{F}_D^{-1}[\mathbf{u}]$ are reordered from $j = N/2 + 1, \dots, N, 1, \dots, N/2$,

$$\hat{\mathcal{F}}_D^{-1}[\mathbf{u}]_j = \begin{cases} \mathcal{F}_D^{-1}[\mathbf{u}]_{j+N/2} & 1 \leq j \leq N/2, \\ \mathcal{F}_D^{-1}[\mathbf{u}]_{j-N/2} & N/2 + 1 \leq j \leq N. \end{cases} \quad (\text{A.2})$$

This is implemented as `ifftshift(ifft(u))` in `FFTW.jl`. Consider the approximation, $j = 1, \dots, N$:

$$\mathcal{F}^{-1}[u](x_j) \approx \frac{1}{2\pi} \int_{-W}^W u(\omega) e^{i\omega x_j} d\omega \approx \frac{\delta}{2\pi} \sum_{n=0}^{N-1} u(\omega_n) e^{i\omega_n x_j}. \quad (\text{A.3})$$

Here we choose the parameters $W \gg 1$ and $N \gg 1$, N even. The points $\omega_n := n\delta - W$, $n = 0, \dots, N-1$, where $\delta := 2W/N$. Substituting in the definition of ω_n , we see that

$$\frac{\delta}{2\pi} \sum_{n=0}^{N-1} u(\omega_n) e^{i\omega_n x_j} = \frac{\delta N e^{-iW x_j}}{2\pi} \left[\frac{1}{N} \sum_{n=0}^{N-1} u(\omega_n) e^{2i x_j W n/N} \right]. \quad (\text{A.4})$$

Define the vector $\mathbf{u}_n = u(\omega_{n-1})$, $n = 1, \dots, N$. Moreover, we fix x_j as

$$x_j := (-N/2 + j - 1) \frac{\pi}{W}, \quad j = 1, \dots, N. \quad (\text{A.5})$$

Then, the right-hand side of (A.4) is equal to

$$\frac{\delta N e^{-iW x_j}}{2\pi} \left[\frac{1}{N} \sum_{n=1}^N \mathbf{u}_n e^{2\pi i(j-1)(n-1)/N} e^{-i\pi(n-1)} \right]. \quad (\text{A.6})$$

By noting that $e^{-i\pi(n-1)} = e^{i\pi(n-1)}$ for $n \in \mathbb{Z}$, then for $1 \leq j \leq N/2$, (A.6) is equal to

$$\frac{\delta N e^{-iWx_j}}{2\pi} \left[\frac{1}{N} \sum_{n=1}^N \mathbf{u}_n e^{2\pi i(j+N/2-1)(n-1)/N} \right], \quad (\text{A.7})$$

and for $N/2 + 1 \leq j \leq N$, (A.6) is equal to

$$\frac{\delta N e^{-iWx_j}}{2\pi} \left[\frac{1}{N} \sum_{n=1}^N \mathbf{u}_n e^{2\pi i(j-N/2-1)(n-1)/N} \right]. \quad (\text{A.8})$$

Hence, by the definition of the shifted IDFT in (A.2), we see that, for $j, n = 1, \dots, N$,

$$\mathcal{F}^{-1}[u](x_j) \approx \frac{\delta N e^{-iWx_j}}{2\pi} \hat{\mathcal{F}}_D^{-1}[\mathbf{u}]_j, \quad (\text{A.9})$$

where $\mathbf{u}_n = u(2W(n-1)/N - W)$, $n = 1, \dots, N$.

B Approximating the appended sum space functions

With a naïve approach, it would take four integrals per interval to approximate the additional functions found in the appended sum space. This setup cost may become prohibitive for a large number of intervals. However, the next proposition reveals that the additional functions on intervals that are translated (and not scaled) are simply translations of the additional functions associated to one reference interval.

Proposition B.1 (Translations of the reference interval). *Consider the interval $I = [a, b]$ and its associated reference interval $I_R = [-(b-a)/2, (b-a)/2]$. Then,*

$$\begin{aligned} v_0^I(x) &= v_0^{I_R}(x - (a+b)/2), & \tilde{u}_{-1}^I(x) &= \tilde{u}_{-1}^{I_R}(x - (a+b)/2), \\ v_1^I(x) &= v_1^{I_R}(x - (a+b)/2), & \tilde{u}_0^I(x) &= \tilde{u}_0^{I_R}(x - (a+b)/2). \end{aligned} \quad (\text{B.1})$$

Proof. The result follows from the identity $\mathcal{F}[f(\diamond + \alpha)](\omega) = e^{i\alpha\omega} \mathcal{F}[f(\diamond)](\omega)$ and a routine calculation. \square

The additional functions on the reference interval are approximated with one integral each. Moreover, all intervals of the same width map to the same reference interval. Hence, the setup of the method only requires four integrals per interval of different width. In particular, if all the intervals have the same width, we only require four integrals in total for the setup, irrespective of the number of intervals used.

References

- [1] R. A. Adams and J. J. Fournier, *Sobolev Spaces*, 2nd ed. Elsevier, 2003, ISBN: 978-0-12-044143-3.
- [2] B. Adcock and D. Huybrechs, “Frames and numerical approximation,” *SIAM Review*, vol. 61, no. 3, pp. 443–473, 2019. DOI: 10.1137/17M1114697.
- [3] —, “Frames and numerical approximation II: Generalized sampling,” *Journal of Fourier Analysis and Applications*, vol. 26, no. 6, pp. 1–34, 2020. DOI: 10.1007/s00041-020-09796-w.
- [4] H. Antil and S. Bartels, “Spectral approximation of fractional PDEs in image processing and phase field modeling,” *Computational Methods in Applied Mathematics*, vol. 17, no. 4, pp. 661–678, 2017. DOI: 10.1515/cmam-2017-0039.
- [5] J. L. Aurentz and L. N. Trefethen, “Chopping a Chebyshev series,” *ACM Transactions on Mathematical Software (TOMS)*, vol. 43, no. 4, pp. 1–21, 2017. DOI: 10.1145/2998442.
- [6] G. R. Baker, X. Li, and A. C. Morlet, “Analytic structure of two 1D-transport equations with nonlocal fluxes,” *Physica D: Nonlinear Phenomena*, vol. 91, no. 4, pp. 349–375, 1996. DOI: 10.1016/0167-2789(95)00271-5.
- [7] D. A. Benson, S. W. Wheatcraft, and M. M. Meerschaert, “Application of a fractional advection-dispersion equation,” *Water Resources Research*, vol. 36, no. 6, pp. 1403–1412, 2000. DOI: 10.1029/2000WR900031.
- [8] V. I. Bogachev and O. G. Smolyanov, *Real and Functional Analysis*. Springer, 2020, ISBN: 978-3-030-38218-6. DOI: 10.1007/978-3-030-38219-3.
- [9] A. Bonito, J. P. Borthagaray, R. H. Nochetto, E. Otárola, and A. J. Salgado, “Numerical methods for fractional diffusion,” *Computing and Visualization in Science*, vol. 19, no. 5, pp. 19–46, 2018. DOI: 10.1007/s00791-018-0289-y.
- [10] A. Bonito, W. Lei, and J. E. Pasciak, “Numerical approximation of the integral fractional Laplacian,” *Numerische Mathematik*, vol. 142, no. 2, pp. 235–278, 2019. DOI: 10.1007/s00211-019-01025-x.
- [11] J. P. Boyd, “A comparison of numerical algorithms for Fourier extension of the first, second, and third kinds,” *Journal of Computational Physics*, vol. 178, no. 1, pp. 118–160, 2002. DOI: 10.1006/jcph.2002.7023.

- [12] O. P. Bruno, Y. Han, and M. M. Pohlman, “Accurate, high-order representation of complex three-dimensional surfaces via Fourier continuation analysis,” *Journal of Computational Physics*, vol. 227, no. 2, pp. 1094–1125, 2007. DOI: 10.1016/j.jcp.2007.08.029.
- [13] L. Caffarelli and J Vázquez, “Regularity of solutions of the fractional porous medium flow with exponent $1/2$,” *St. Petersburg Mathematical Journal*, vol. 27, no. 3, pp. 437–460, 2016. DOI: 10.1090/spmj/1397.
- [14] B Carmichael, H Babahosseini, S. Mahmoodi, and M Agah, “The fractional viscoelastic response of human breast tissue cells,” *Physical Biology*, vol. 12, no. 4, p. 046001, 2015. DOI: 10.1088/1478-3975/12/4/046001.
- [15] D. Chae, A. Córdoba, D. Córdoba, and M. A. Fontelos, “Finite time singularities in a 1D model of the quasi-geostrophic equation,” *Advances in Mathematics*, vol. 194, no. 1, pp. 203–223, 2005. DOI: 10.1016/j.aim.2004.06.004.
- [16] S. Chen, J. Shen, and L.-L. Wang, “Laguerre functions and their applications to tempered fractional differential equations on infinite intervals,” *Journal of Scientific Computing*, vol. 74, no. 3, pp. 1286–1313, 2018. DOI: 10.1007/s10915-017-0495-7.
- [17] J. W. Cooley and J. W. Tukey, “An algorithm for the machine calculation of complex Fourier series,” *Mathematics of Computation*, vol. 19, no. 90, pp. 297–301, 1965. DOI: 10.2307/2003354.
- [18] A. Córdoba, D. Córdoba, and M. A. Fontelos, “Integral inequalities for the Hilbert transform applied to a nonlocal transport equation,” *Journal de Mathématiques Pures et Appliquées*, vol. 86, no. 6, pp. 529–540, 2006. DOI: 10.1016/j.matpur.2006.08.002.
- [19] M. D’Elia, Q. Du, C. Glusa, M. Gunzburger, X. Tian, and Z. Zhou, “Numerical methods for nonlocal and fractional models,” *Acta Numerica*, vol. 29, pp. 1–124, 2020. DOI: 10.1017/S096249292000001X.
- [20] E. Di Nezza, G. Palatucci, and E. Valdinoci, “Hitchhiker’s guide to the fractional Sobolev spaces,” *Bulletin des Sciences Mathématiques*, vol. 136, no. 5, pp. 521–573, 2012. DOI: 10.1016/j.bulsci.2011.12.004.
- [21] T. A. Driscoll, N. Hale, and L. N. Trefethen, *Chebfun Guide*, 2014.
- [22] Q. Du, *Nonlocal Modeling, Analysis, and Computation*. SIAM, 2019, ISBN: 978-1-61197-561-1. DOI: 10.1137/1.9781611975628.

- [23] N. Hale and S. Olver, “A fast and spectrally convergent algorithm for rational-order fractional integral and differential equations,” *SIAM Journal on Scientific Computing*, vol. 40, no. 4, A2456–A2491, 2018. DOI: 10.1137/16M1104901.
- [24] Y. Hatano and N. Hatano, “Dispersive transport of ions in column experiments: An explanation of long-tailed profiles,” *Water Resources Research*, vol. 34, no. 5, pp. 1027–1033, 1998. DOI: 10.1029/98WR00214.
- [25] R. Hunt, B. Muckenhoupt, and R. Wheeden, “Weighted norm inequalities for the conjugate function and Hilbert transform,” *Transactions of the American Mathematical Society*, vol. 176, pp. 227–251, 1973. DOI: 10.1090/S0002-9947-1973-0312139-8.
- [26] D. Huybrechs, “On the Fourier extension of nonperiodic functions,” *SIAM Journal on Numerical Analysis*, vol. 47, no. 6, pp. 4326–4355, 2010. DOI: 10.1137/090752456.
- [27] W. R. Inc., *Mathematica, Version 13.1*, Champaign, IL, 2022.
- [28] M. Johansson, “The Hilbert Transform,” M.S. thesis, Växjö University, Suecia, 1999.
- [29] F. W. King, *Hilbert Transforms: Volume 1*, ser. Encyclopedia of Mathematics and its Applications. Cambridge University Press, 2009, vol. 1. DOI: 10.1017/CB09780511721458.
- [30] M. Kwaśnicki, “Ten equivalent definitions of the fractional Laplace operator,” *Fractional Calculus and Applied Analysis*, vol. 20, no. 1, pp. 7–51, 2017. DOI: 10.1515/fca-2017-0002.
- [31] H. Li, R. Liu, and L.-L. Wang, “Efficient Hermite spectral-Galerkin methods for nonlocal diffusion equations in unbounded domains,” *Numerical Mathematics: Theory, Methods and Applications*, 2022. DOI: 10.4208/nmtma.0A-2022-0007s.
- [32] A. Lischke, G. Pang, M. Gulian, F. Song, C. Glusa, X. Zheng, Z. Mao, W. Cai, M. M. Meerschaert, M. Ainsworth, *et al.*, “What is the fractional Laplacian? A comparative review with new results,” *Journal of Computational Physics*, vol. 404, p. 109009, 2020. DOI: 10.1016/j.jcp.2019.109009.
- [33] Z. Mao and J. Shen, “Hermite spectral methods for fractional PDEs in unbounded domains,” *SIAM Journal on Scientific Computing*, vol. 39, no. 5, A1928–A1950, 2017. DOI: 10.1137/16M1097109.
- [34] SumSpaces.jl as used in ‘A sparse spectral method for fractional differential equations in one-spatial dimension’, version 0.0.1, 2022. DOI: 10.5281/zenodo.7185131.

- [35] `SumSpacesMathLink.jl` as used in ‘A sparse spectral method for fractional differential equations in one-spacial dimension’, version 0.0.1, 2022. DOI: 10.5281/zenodo.7185106.
- [36] F. W. J. Olver, A. B. Olde Daalhuis, D. W. Lozier, B. I. Schneider, R. F. Boisvert, C. W. Clark, B. R. Miller, B. V. Saunders, H. S. Cohl, and M. A. McClain, *NIST Digital Library of Mathematical Functions*, <http://dlmf.nist.gov/>, Release 1.1.4 of 2022-01-15.
- [37] S. K. Pichorides, “On the best values of the constants in the theorem of M. Riesz, Zygmund and Kolmogorov,” *Studia Mathematica*, vol. 44, no. 2, pp. 165–179, 1972.
- [38] J. Rauch, *Partial Differential Equations*. Springer New York, NY, 1991, vol. 1, ISBN: 978-0-387-97472-9. DOI: 10.1007/978-1-4612-0953-9.
- [39] C. Sheng, J. Shen, T. Tang, L.-L. Wang, and H. Yuan, “Fast Fourier-like mapped Chebyshev spectral-Galerkin methods for PDEs with integral fractional Laplacian in unbounded domains,” *SIAM Journal on Numerical Analysis*, vol. 58, no. 5, pp. 2435–2464, 2020. DOI: 10.1137/19M128377X.
- [40] G. W. Stewart, *Afternotes Goes to Graduates School*. SIAM, 1998, ISBN: 978-0-89871-404-3. DOI: 10.1137/1.9781611971422.
- [41] T. Tang, L.-L. Wang, H. Yuan, and T. Zhou, “Rational spectral methods for PDEs involving fractional Laplacian in unbounded domains,” *SIAM Journal on Scientific Computing*, vol. 42, no. 2, A585–A611, 2020. DOI: 10.1137/19M1244299.
- [42] T. Tang, H. Yuan, and T. Zhou, “Hermite spectral collocation methods for fractional PDEs in unbounded domains,” *Communications in Computational Physics*, vol. 24, no. 4, pp. 1143–1168, 2018. DOI: 10.4208/cicp.2018.hh80.12.
- [43] E. C. Titchmarsh *et al.*, *Introduction to the theory of Fourier integrals*. Clarendon Press Oxford, 1948, vol. 2, ISBN: 9780828403245.
- [44] B. E. Treeby and B. T. Cox, “Modeling power law absorption and dispersion for acoustic propagation using the fractional Laplacian,” *The Journal of the Acoustical Society of America*, vol. 127, no. 5, pp. 2741–2748, 2010. DOI: 10.1121/1.3377056.
- [45] T. Trogdon and S. Olver, *Riemann–Hilbert Problems, Their Numerical Solution, and the Computation of Nonlinear Special Functions*. SIAM, 2015, ISBN: 978-1-611974-19-5.
- [46] J. L. Vázquez, “Asymptotic behaviour for the fractional heat equation in the Euclidean space,” *Complex Variables and Elliptic Equations*, vol. 63, no. 7-8, pp. 1216–1231, 2018. DOI: 10.1080/17476933.2017.1393807.

- [47] G. N. Watson, *A Treatise on the Theory of Bessel Functions*. The University Press, 1922, vol. 3, ISBN: 978-0-521-09382-8.